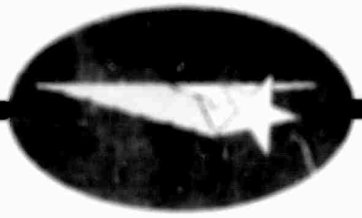

Unclassified
Security Classification

DOCUMENT CONTROL DATA - R & D

(Security classification of title, body of abstract and indexing annotation must be entered when the overall report is classified)

1. ORIGINATING ACTIVITY (Corporate author) Lockheed Palo Alto Research Laboratory	2a. REPORT SECURITY CLASSIFICATION Unclassified 2b. GROUP

3. REPORT TITLE

Satellite Data Analysis to Investigate the Horizontal Ion Density Gradients in the Lower Ionosphere

4. DESCRIPTIVE NOTES (Type of report and inclusive dates)

Final Technical Report, 1 May 1970 through 31 May 1971

5. AUTHOR(S) (First name, middle initial, last name)

Gerald W. Sharp, Kent K. Harris, R. D. Sharp, W. C. Knudsen and Richard G. Johnson

6. REPORT DATE	7a. TOTAL NO. OF PAGES	7b. NO. OF REFS
May 1971	83	8

8a. CONTRACT OR GRANT NO.	9a. ORIGINATOR'S REPORT NUMBER(S)
N00014-70-C-0324 b. PROJECT NO.	LMSC/D177361
c.	9b. OTHER REPORT NO(S) (Any other numbers that may be assigned this report)
d.	--

10. DISTRIBUTION STATEMENT

This document has been approved for public release and sale; its distribution is unlimited.

11. SUPPLEMENTARY NOTES	12. SPONSORING MILITARY ACTIVITY
	Office of Naval Research Advanced Research Projects Agency

13. ABSTRACT

This final report is on the analysis of the data obtained from a satellite measurement program to investigate the characteristics and causes of horizontal ion density gradients in the F-region ionosphere. Data from the orbits prior to 225 of the OVI-18 satellite are analyzed here. The OVI-18 satellite was launched on 18 March 1969 into a polar orbit with apogee at 590 km and perigee at 469 km. Although the vehicle failed to achieve its desired earth-orientation, much valuable ion, electron and energetic particle data were obtained. Many gradients were observed in the ion density, some of which correlated with energetic particle precipitation in the auroral zones. It is concluded that precipitated particles in the night auroral zones give rise to significant ionization gradients at low altitudes and that these effects, although reduced in magnitude, are also seen at altitudes near 500 km, well above the F_2 peak in ionization.

DD FORM 1 NOV 68 1473

Unclassified
Security Classification

14 KEY WORDS	LINK A		LINK B		LINK C	
	ROLE	WT	ROLE	WT	ROLE	WT
Ionosphere						
Ion Density Gradients						
Ionospheric Structure						
Satellite Data						
OVI-18 Satellite						

Final Report

Contract N00014-70-C-0324

Satellite Data Analysis to Investigate the Horizontal Ion Density Gradients in the Lower Ionosphere

Contractor:	Lockheed Missiles and Space Company
Project Leader:	Dr. G. W. Sharp (415-324-3311, Extension 45353)

Effective Date of Contract:	1 May 1970
Contract Expiration Date:	28 February 1971
Amount of Contract:	CPFF $51,800
Cost Code:	0F10K18

Sponsored by Advanced Research Projects Agency (ARPA)

Order No. 215

31 March 1971

Table of Contents

List of Figure Captions

List of Tables

Section 1

INTRODUCTION

Section 1

INTRODUCTION

This is the final report for a data analysis program applied to a satellite that was designed to investigate the characteristics and causes of horizontal ion density gradients in the F-region ionosphere. The satellite instrument package designed and developed under Contract NOnr-[illegible](00) for investigation of the extent and causes of horizontal ionospheric structure was successfully launched on the OV1-18 satellite on 18 March 1969 into a 99° inclination orbit with a 990 km apogee and a [illegible] km perigee. All of the 13 instruments operated successfully on orbit and provided valuable data. After 18 months of on-orbit operation, 11 of the instruments were still providing excellent data. The satellite performance was good except for the attitude stabilization which was never achieved. The satellite has been turned off since September, 1970, due to the failure of the on-board tape recorder. As a result of the satellite instabilities, the data analysis procedures are more complex and the spatial coverage will be restricted for some of the measured parameters.

Preliminary data reduction and analysis has been achieved for selected orbits up to revolution 1500. The quality of the data is excellent and the large variations in the solar and geophysical conditions during the period provide the desired opportunities to investigate the ionospheric characteristics for a wide variety of conditions. The emphasis placed on the analysis effort under the present contract was with the data acquired prior to satellite revolution number 225 since the instrument to measure the positive ion density and temperature did not function properly on later revolutions.

The ionosphere is frequently characterized by its ability to absorb, refract, or reflect electromagnetic irradiations. These characteristics are clearly important to terrestrial and space communications networks and to radar tracking systems, particularly over-the-horizon tracking systems. In addition, the ionosphere plays an important role in the ability to detect, locate, and characterize nuclear detonations by means of the electromagnetic signals produced by the detonations. Changes in the natural ionosphere density and composition are also produced by nuclear detonations in or near the ionosphere, and identification of the perturbed ionization can serve as a means of detection and characterization of the nuclear device.

It is well known that nuclear detonations in the earth's magnetosphere produce strong electromagnetic signals, particularly in the low-frequency range. Detection of these signals and measurements of their characteristics provide a means of identifying, locating, and characterizing a nuclear detonation. Electromagnetic signals from nuclear detonations have frequently been observed at large distances from the point of detonation as a result of the propagation of the signals through the ionosphere or within the earth-ionosphere cavity. The intensity, time dependence, and frequency composition of these signals at remote distances are strong functions of the characteristics of the ionosphere. At present, our limited knowledge of the structure of the ionosphere continues to limit our ability to determine the electromagnetic source characteristics from measurements on the signals received at distant stations.

Prior to the initiation of the present program, large horizontal gradients in the ion density near the region of maximum density in the

F-region (300-350 km) had been observed by the Lockheed Upper Atmospheres Group[1] with satellite instrumentation during a 4-day flight in November 1963. Some of the gradients persisted from day to day and were generally aligned with the magnetic field. These data, coupled with earlier data from the Alouette topside sounder, indicated that a nighttime trough of low ion density might be present at all altitudes on the equatorial side of the auroral zones. The data also showed that the ion density gradients on the nightside of the earth in the region of the polar auroral zones were related to the low-energy precipitated particle fluxes in those regions. Horizontal gradients were also observed in the South Atlantic anomaly region and they appeared to be directly associated with the artificial radiation belt and at times with the Van Allen radiation belt[2]. More detailed reports of the early Lockheed and Alouette results have subsequently been published elsewhere[3,4].

The present program was undertaken to improve our understanding of the horizontal ion density gradients. The major goals of the program are 1) to investigate the vertical extent of the type of horizontal ion density gradients observed in November 1963, 2) to study the local time dependence and other long-term and short-term variations of the observed structure and 3) to investigate the role of the energetic particle fluxes in providing the ion density gradients.

Initially, two satellite flights were planned. One was to be flown above the F-region peak density (400-500 km) and one below the peak (250-300 km). The satellite experiment that has been completed and is reported here was flown above the F-peak.

A complete list of the instruments flown on OV1-18 under the heading of HIGLO (Horizontal Ion Density Gradients in the Lower Atmosphere) is given in Table 1.1. Included in the table is a brief statement of the measurement made by each instrument. A rather complete description of each of the instruments, their calibration and operation, is included in the Final Report of Investigations of Horizontal Ion Density Gradients[5] and will not be repeated here.

	Instrument	Measurement
1.	Ion Energy Analyzer	Ion density and temperature
2.	Epithermal Electron Analyzer	Epithermal electron energy distribution from 0 to 130 eV.
3.	Cylindrical Langmuir Probe	Ambient electron density and temperature.
4.	Electrostatic Analyzer	Mass and energy distribution of energetic ions.
5.	0 Multi-Channel Particle Analyzer	Proton and electron energy distribution along the zenith.
6.	90 Multi-Channel Particle Analyzer	Proton and electron energy distribution 90° to the zenith.
7.	55 Multi-Channel Particle Analyzer	Proton and electron energy distribution 55° to the zenith.
8.	Proton Hydrogen Analyzer	Ratio of energetic Helium ions to protons.
9.	Total Energy Proton Sensor #1	Total proton energy flux above 4 keV threshold.
10.	Total Energy Proton Sensor #2	Total electron energy flux above 21 keV threshold.
11.	Angular Distribution Instrument	Angular distribution of electrons with total energy flux above two thresholds, 0.2 and 1.2 keV.
12.	Penetrating Radiation Monitor	Highly penetrating particles in the radiation belts and the polar cap region.
13.	Electric Field Probe	Proton and electron energy distribution along the nadir.

Table 1.1 HIGLO Instruments and their Measurement

Section 1

REFERENCES

1. Sharp, G. W., T. J. Crowther and C. W. Gilbreth, "Some Recent Ion Concentration Measurements Obtained from a Polar Orbiting Satellite," Trans. Am. Geophys. U., 45, 87-88 (1964).

2. Sharp, G. W., W. L. Imhof and R. G. Johnson, "Direct Evidence for Corpuscular Radiation Effects on the Ionosphere in the Southern Anomaly Region," COSPAR Conference, Buenos Aires, May 1965; Space Research VI, North-Holland Publishing Co., 1966.

3. Muldrew, D. B., "F-Layer Ionization Troughs Deduced from Alouette Data," J. Geophys. Res., 70, 2635 (1965).

4. Sharp, G. W., "Midlatitude Trough in the Night Ionosphere," J. Geophys. Res., 71, 1345 (1966).

5. Sharp, G. W., R. D. Sharp and R. G. Johnson, "Investigation of Horizontal Ion Density Gradients," Final Report for Contract NOnr 4969(00), Lockheed Missiles and Space Company, LMSC/L-39-70-1 (unclassified), June 1970.

Section 2

VEHICLE EPHEMERIS AND ATTITUDE DETERMINATION

Section 2

VEHICLE EPHEMERIS AND ATTITUDE DETERMINATION

2.1 Ephemeris Determination

The ephemeris program routinely used in conjunction with the data analysis makes use of the inertial coordinates provided on an hourly basis by ENT Air Force Base, Colorado. The program represents a modification of one previously written at LMSC. In addition to providing the geographic coordinates once every ten seconds, several other important quantities are computed. Subroutines are incorporated for calculating various quantities relating to the earth's magnetic field: B,L, the invariant latitude, K_{Min}, altitude of the conjugate point, and the auroral time. For a typical orbit acquisition approximately two to three minutes of 1108 computer time is required.

The validity of the ephemeris program is checked on a given orbit by comparison of current output of the solar arrays to the times of transition from sunlight to darkness as calculated by the ephemeris program. This test can indicate accuracy of 3 to 5 seconds of time in the ephemeris. Another validity check involves comparisons between the magnetic field strengths measured with the magnetometer and those calculated from the geographic position and the earth's magnetic field model. This technique will readily indicate the existence of large errors in the ephemeris but is not competitive with the light sensors in regard to accuracy. The response of the PRM instrument to the four crossings of the outer radiation belt on each orbit also serves as an indication of any gross ephemeris errors.

As a result of the foregoing tests it was discovered that the ephemeris values supplied by ENT Air Force Base were in serious error for the first 388 orbits. For example, on orbit 388 the light sensor indicated a time equivalent error of 125 seconds. Upon further checking, a sudden step function in the satellite position, as derived from the ephemeris cards supplied by ENT, was uncovered. It is now generally agreed that the tracking data used were for another object near the OV1-18 satellite. For six months personnel at ENT tried without success to generate a correct ephemeris for the first 388 orbits. As a result of their difficulties it became necessary to obtain valid ephemeris for orbits less than 388 by utilizing an LMSC program to run "backward" in time for about 20 days to cover the earlier orbits. In this way it was possible to generate ephemeris with adequate accuracy for all orbits up to orbit number 388. The accuracy of the ephemeris was tested for revolution 6007 by comparing the calculated positions with those measured with radar techniques by Dr. A. Freed at Lincoln Laboratory, Massachusetts Institute of Technology. The calculated and measured positions were found to agree within five kilometers.

2.2 Attitude Determination

The most difficult task associated with this data analysis effort was the development of techniques to establish the vehicle attitude with respect to the vehicle velocity vector. The need arising from the fact the gravity-gradient stabilization booms were never properly deployed which meant that the OV1-18 satellite never achieved the desired three-axis, earth-centered stabilization.

Initially, the satellite instability manifested itself as a relatively slow tumble with a rate of 0.01 per minute or approximately one complete revolution per orbit. The tumble rate slowly increased in an approximately linear manner to 0.28 revolutions per minute as shown in Figure 2-1 until mid-September 1969 when one or more of the booms apparently came free of the satellite. At this point, the tumble rate increased more dramatically to a maximum value of 0.48 revolution per minute and then slowly decreased to the present value of approximately 0.40 revolution per minute. The tumble rate was continuously monitored along the three principle vehicle axes by a tri-axis magnetometer.

When the vehicle is in the sun, its attitude can be obtained from the sun sensor and magnetometers on board the vehicle. A first step, then, was to establish the residual offsets of the magnetometers so that their readings can be compared to a model of the earth's magnetic field. In addition, all the energetic particle measuring instruments required an accurate knowledge of their orientation with respect to the earth's magnetic field. The calculated orientation of the instruments is very sensitive to the corrections to the measured field which must be applied because of vehicle fields. If one assumes that the vector offset field is constant in the frame of the satellite, it can be determined by comparing the measured field with the field expected on the basis of established field models. If we define the quantities

$$B_0 = \text{Model field}$$

$$B_M = \text{Measured field}$$

$$\Delta_B = B_M - B_0$$

an offset field will show up as a quasi-periodic modulation of ΔB with a

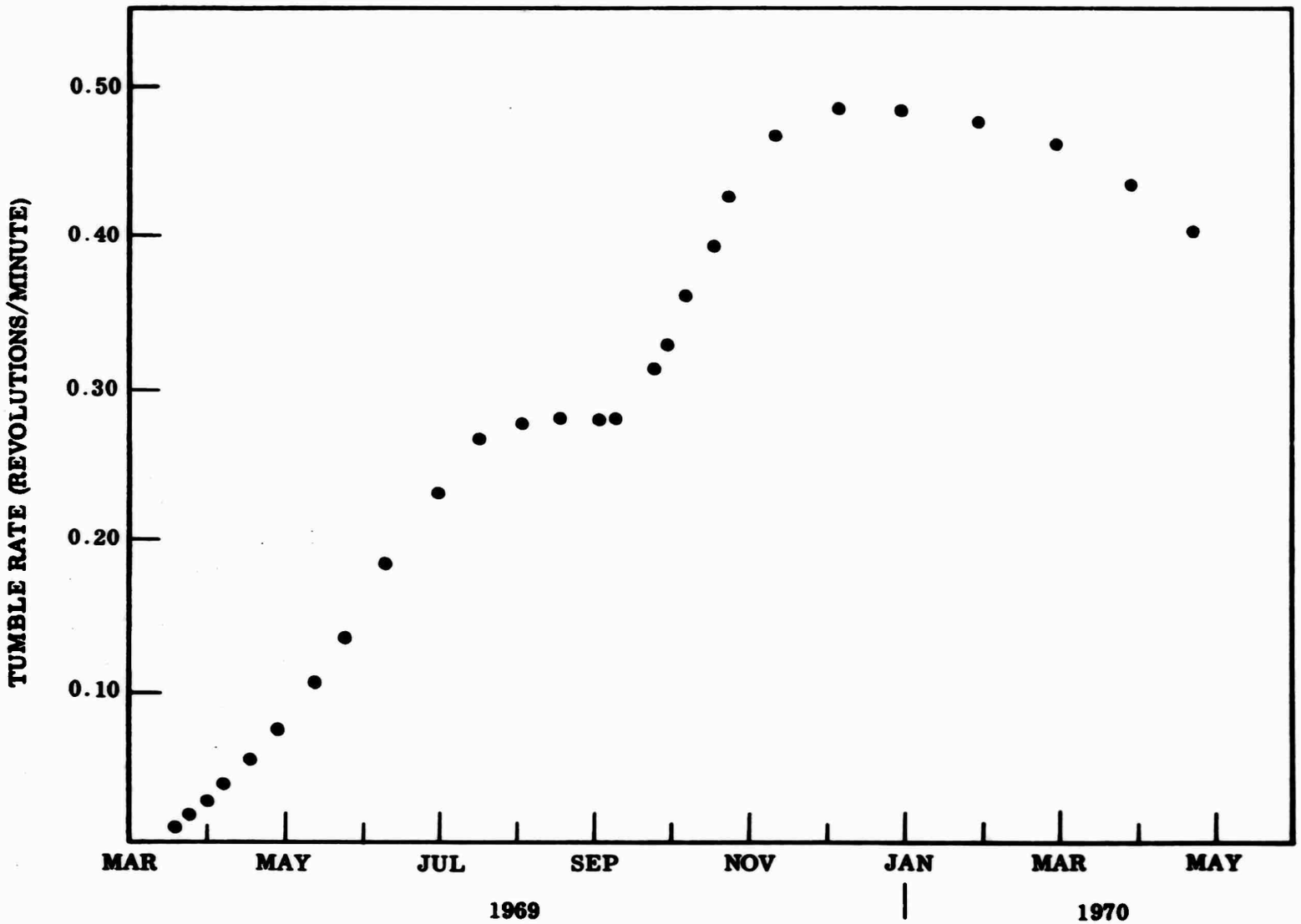

Figure 2-1 Tumble Rate of Satellite During the Active Life of OVI-18

period equal to the spin period of the satellite. This is clearly demonstrated in Figure 2-2. The modulation is not a simple sinusoidal function because the vector orientation of the vehicle offset field and the geomagnetic field varies in a complex way as the satellite tumbles.

If one assumes a possible vehicle offset field with vector components $-C_j$ where j denotes the coordinate axis and an error in the calibration scale factor of (A_2-1) for each axis, we can relate the true (model) field B_j to the measured field b_j in the following way.

$$B_j(t) = A_j[b_j(t) + C_j]$$

If the vehicle orientation were independently known, one could calculate $B_j(t)$ from the model and evaluate C_j and A_j from a best fit. However, without prior knowledge of the vehicle orientation we must base our corrections on the discrepancy in the total field.

$$B(t) = \left(A_1^2[b_1(t) + C_1]^2 + A_2^2[b_2(t) + C_2]^2 + A_3^2[b_3(t) + C_3]^2\right)^{\frac{1}{2}}$$

To evaluate C_1, we first choose cases where $b_2(t_i) = b_3(t_i) = 0$, in which case we can write

$$B_i = \left\{A_1^2(b_{1i}+C)^2\left[1+\left(\frac{A_2C_2}{A_1[b_{1i}+C_1]}\right)^2 + \left(\frac{A_3C_3}{A_1[b_{1i}+C_1]}\right)^2\right]\right\}^{\frac{1}{2}}$$

where we have used the notation $B(ti) = B_i$ and $b_1(t_i) = b_{1i}$. If, as is shown to be the case, the corrections are small compared with the total field, we can drop the second order terms and obtain

$$B_i \cong A_1(b_{1i} + C_1).$$

From two such cases, one where $b_{1i} > 0$ and the other where $b_{1k} < 0$, we have

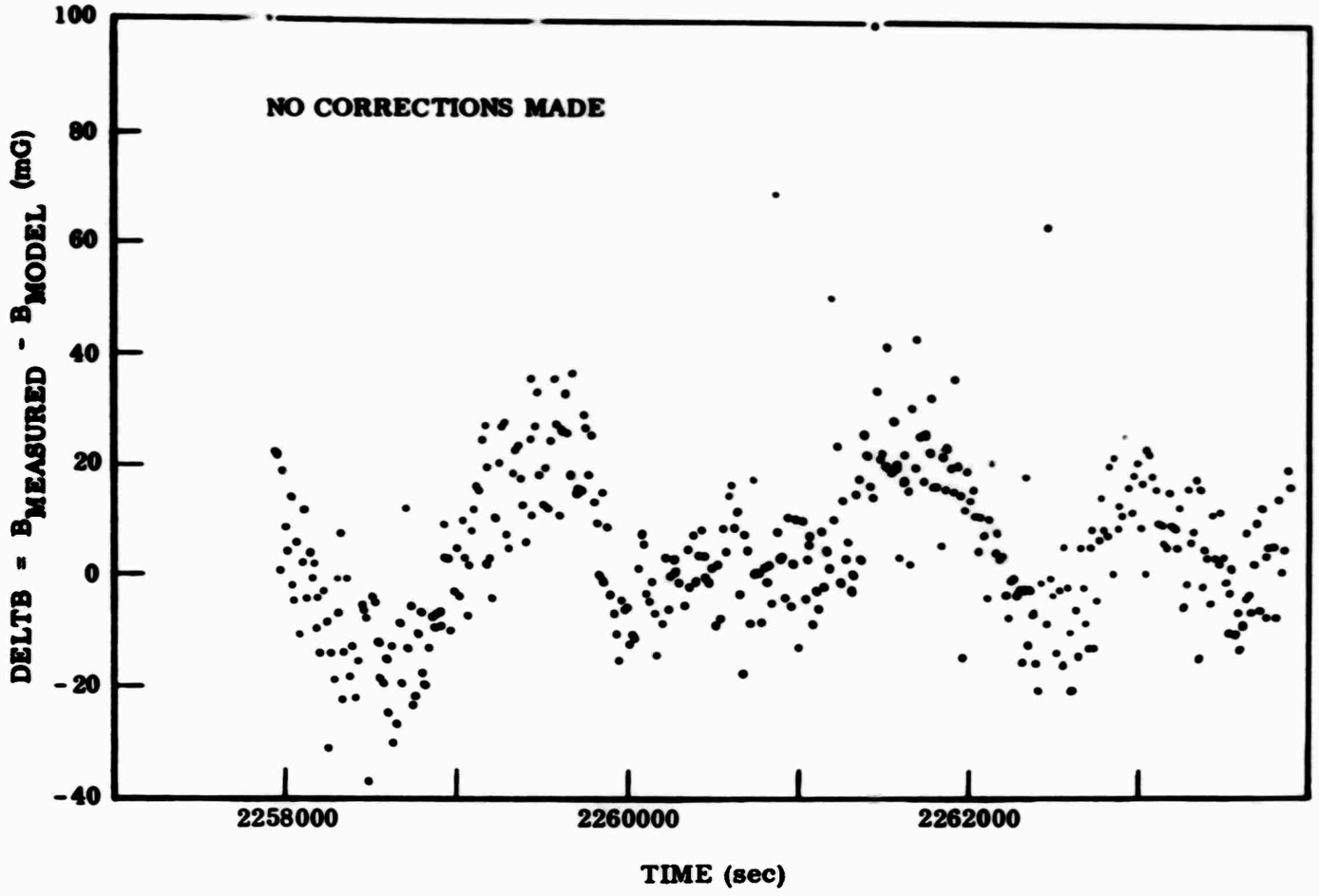

Figure 2-2 The Effects of Magnetic Field Offsets on the Uncorrected Magnetometer Data

$$B_k = -A_1(b_{1k}+C_1) = A_1(|b_{1k}| - C_1)$$

$$B_i = A_1(b_{1k}+C_1).$$

Then

$$A_1 = \frac{B_i + B_k}{b_{1i} + |b_{1k}|}$$

$$C_1 = \frac{B_i|b_{1k}| - B_k b_{1i}}{B_i + B_k} .$$

Similar results are obtained for A_2, C_2 and A_3, C_3 by choosing suitable cases where $b_1 = B_3 = 0$ and $b_1 = b_2 = 0$, respectively.

A statistical analysis of all available data for these cases lead to the following results.

$$C_R = -19 \text{ mG}$$

$$C_V = -8 \text{ mG}$$

$$C_Z = -9 \text{ mG}$$

$$A_R \cong A_V \cong A_Z \cong 1.02$$

Figure 2-3 is the same data shown in Figure 2-2 after correcting for the offset field, but not applying the scale factor. The solid line shows where the zero line would be if a scale correction A = 1.025 were applied to the data. It is obvious that the periodic modulation has been eliminated. The remaining scatter results primarily from the finite resolution of the telemetry system and general noise.

With the vehicle magnetometer offsets established, the next step was to add the information from the solar sensor to the magnetometer information and establish the vehicle attitude. It requires two non-colinear

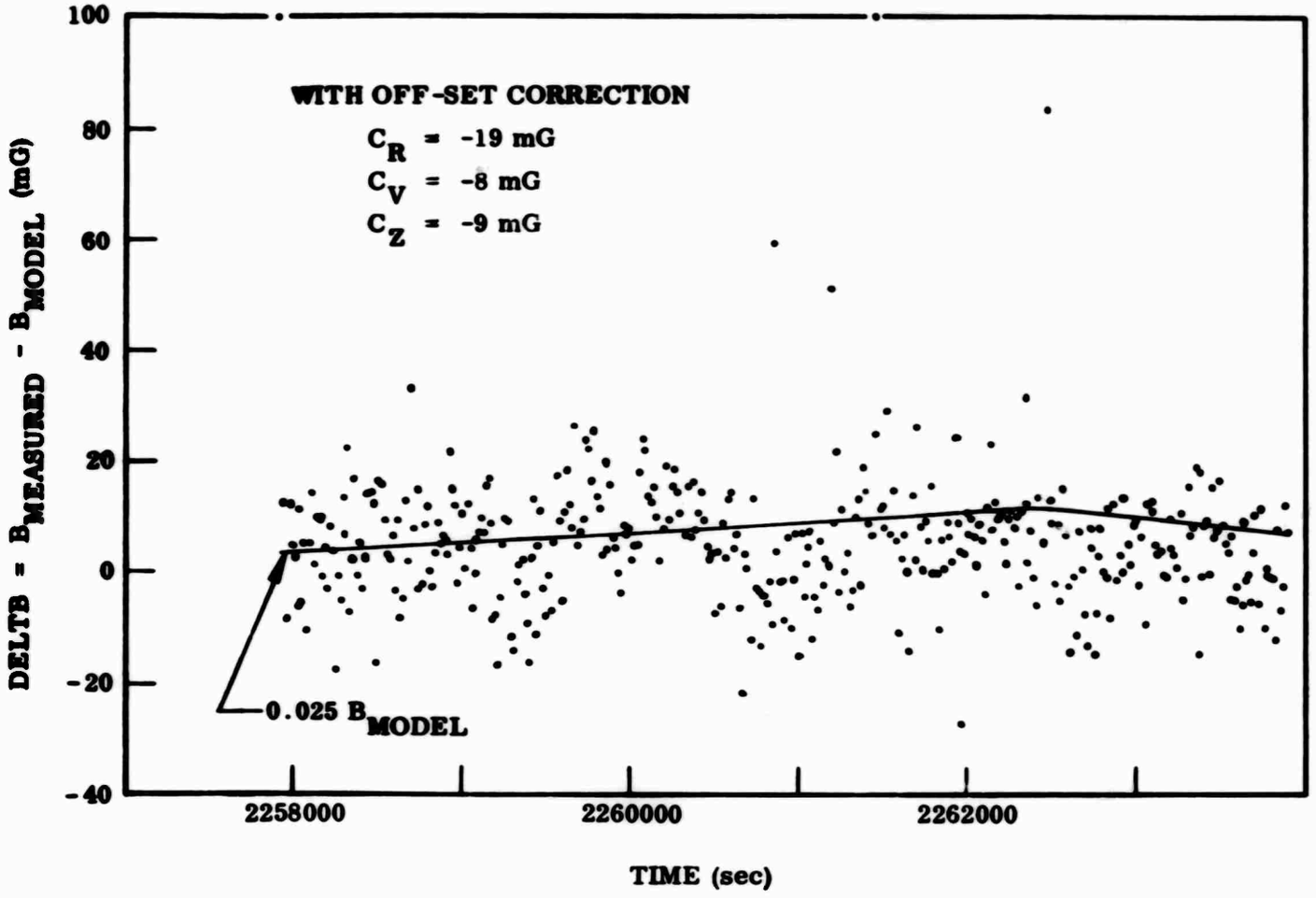

Figure 2-3 The Effects of Magnetic Field Offsets on the Corrected Magnetometer Data

vectors to uniquely define the spacecraft attitude. The three axis magnetometer provides one vector and the sum sensor supplies the other (when the vehicle is sunlit). A program was developed which determined the vehicle orientation in space in terms of the three Euler angles that describe the general rotations of the Space Craft Coordinate System with respect to the fixed earth centered-inertial coordinate system. This program was based on a program kindly supplied to us by the Aerospace Corporation which they had developed for this same purpose on earlier OVI satellites. Orbit-attitude tapes were generated for the sunlit portion of the orbits prior to number 225 using this computer program.

During the non-sun illuminated portion of an orbit the attitude of the satellite cannot be determined in the straight forward manner described above. As mentioned above, it requires two non-colinear vectors to uniquely define the spacecraft attitude, and during the "night-time" portion of the orbit only the magnetic field vector from the magnetometers is available. Since the Ion Energy Analyzer (IEA) is sensitive to the angle the velocity vector makes with the normal to the plane of its sensor, and since four sensor elements were employed and distributed effectively coplanar in the spacecraft it has been possible to extrapolate the Euler angles into the nighttime sector. The Euler angle extrapolations were accomplished by fitting the measured magnetic field vector obtained by the spacecraft to the model magnetic field vector. All sets of Euler angles compatible with this vector fit were used to calculate the expected signals to each of the four IEA sensors. The set of Euler angles which gave the "best fit" to the measured signals from the IEA was chosen to be the correct set.

From the above procedures, it is felt that the Euler angles and hence the spacecraft attitude have been determined to a reasonable accuracy for most orbits prior to number 225. Apart from the expense in time and money required to develop these programs for vehicle attitude, the most significant effect that the lack of vehicle stability has produced is a reduction in the fraction of time spent observing (or measuring) a given phenomena. That is, during significant portions of some orbits the instruments are not looking in a favorable direction, as will be seen in the next section when the data from the ion energy analyzer is presented. However, since each instrument orientation with respect to either the vehicle velocity vector or the earth's geomagnetic field is known at all times, extremely valuable information has come from the data when the vehicle orientation is favorable.

Section 3

ION CONCENTRATION

Section 3

Ion Concentration

Ion concentration data obtained from the Ion Energy Analyzer is presented in Figures 3-1 to 3-8. The ion concentration is plotted as a function of universal time (in seconds). At each 500 sec time interval, the corresponding values of vehicle altitude, geographic latitude and geomagnetic L parameter are also given. Indicated on each figure is the location of the point of transition from sunlight to darkness. On most figures the location of the auroral regions are shown by the area marked with an "A." These regions were determined from particle precipitions as measured by other instrumentation carried aboard the vehicle. On those figures where auroral zones are not indicated, there were no precipitated particles observed.

Large data gaps appear in the data. Small data gaps also appear, and are frequently filled in with a broken line. Thus where broken lines appear in the data the exact shape of the ion density profile is not presented. The broken line does signify the general trend of the data, however. These data gaps, both large and small, are the result of the orientation of the vehicle. During the data gap periods the vehicle was in an unfavorable orientation for accurate ion concentration analysis.

The vehicle, originally designed to be operated in a stable earth-oriented mode, assumed a spinning-tumbling mode as described in the previous section. The IEA required a look angle into the velocity vector of less than 50°. Preflight dynamical analysis indicated that stabilized orientation might not be achieved, therefore, four separate sensor elements

were positioned co-planar with the Roll-Zee plane of the vehicle. One sensor was positioned with its symmetry axis along the positive zee axis of the vehicle, another was positioned with its symmetry axis along the negative zee axis. The other two sensor elements were positioned with their symmetry axes making $+50^{\circ}$ and -50°, respectively, with the negative zee axis. With this positioning of the 4 sensor elements nearly all orientations for a spinning vehicle, with the spin vector normal to the Roll-Zee plane, would place the velocity vector within an acceptable angle with at least one of the sensor elements. Unfortunately, it appears that the vehicle also executed a slow tumbling motion. The complex motion of the vehicle therefore frequently caused the velocity vector to lie outside of the acceptable entrance cones of any of the instrument sensors. On these occasions, large blocks of data were rendered greatly suspect and were therefore discarded.

During the period of observation, the magnetosphere was highly disturbed. One of the most intense magnetic storms of the decade was recorded during the period from March 19, 1969, to March 25, 1969. On four of these five successive nights, red arcs were observed at the Richland Washington observation site. One must, therefore, expect that the disturbance caused by the magnetic storm will manifest itself in the characteristics of the ionosphere.

A curious feature of the data is that the expected diurnal effect on the ion concentration data does not appear to be present. The ion concentration measured on the nightside of the orbit is generally just as large as the ion concentration observed on the dayside of the orbit. It may very well be that under these disturbed conditions, a significant energy deposit occurs in the night time region that maintains the high

ionization levels for that sector. Coupled into the diurnal effect is an altitude effect, however, in that the altitude on the night sector is somewhat lower than the altitude on the day sector.

The most striking feature of the data is the number and magnitude of ion concentration gradients. These gradients are present both in the sunlight and during the nighttime. The gradients are however usually more pronounced during the night. Frequently, the total change in ion concentration in one of the night time gradients is about an order of magnitude, and on occasions will be as great as two orders of magnitude. However, these latter cases are usually associated with the main night time ion density trough.

In most cases the night time main trough is observed. However, its character is rather variable. The depth of the trough varies from perhaps a factor of five to as much as two orders of magnitude. The width of the trough is at times extremely narrow while at other times is rather broad. The steepness of the walls of the trough also shows marked changes from one trough to the next.

Peaks in the ion concentration data are also readily observed. The highest peaks in the night time sector are found to occur quite regularly at L values of 1.1. The fact that the largest peaks occur at L = 1.1 may be due however to an altitude effect. The altitude is near its minimum at L = 1.1. Nevertheless, it is significant that peaks in the ion concentration occur at night and that they are repetitive in their location with respect to the geophysical parameter L. Concentration peaks are also found to occur on the dayside of the orbit although less frequently and perhaps less dramatically than those that occur at night. The dayside

peaks are usually not as sharp nor are they as pronounced as those on the night side. Generally the dayside peaks are rather broad and do not stand out significantly above the average concentration when compared to the nightside peaks. The maxima of the dayside peaks consistently occur at L values near 1.2 and at positions in the orbit very near apogee.

The dayside ion concentration shows a very significant latitudinal dependence. The lower ion concentration values occur at the high latitude regions, even when those high latitude regions are at the lower altitudes of the orbits. The larger ion concentration values occur generally near the equator and at the higher altitudes. Upon correcting for the altitude dependence, the latitude dependence of ion concentration would be even more pronounced.

The general trend of the nighttime ion concentration also indicates a latitude dependence, with increasing values as the vehicle approaches the equatorial regions. The conclusion for the nighttime latitude dependence may not be made as strongly as that for the dayside in that the height profile over the night sector shows a decrease as latitude decreases and is near minimum at the equator. Therefore, the ion concentration increase measured on the nightside as the vehicle approaches the equator may be in part due to the altitude decrease.

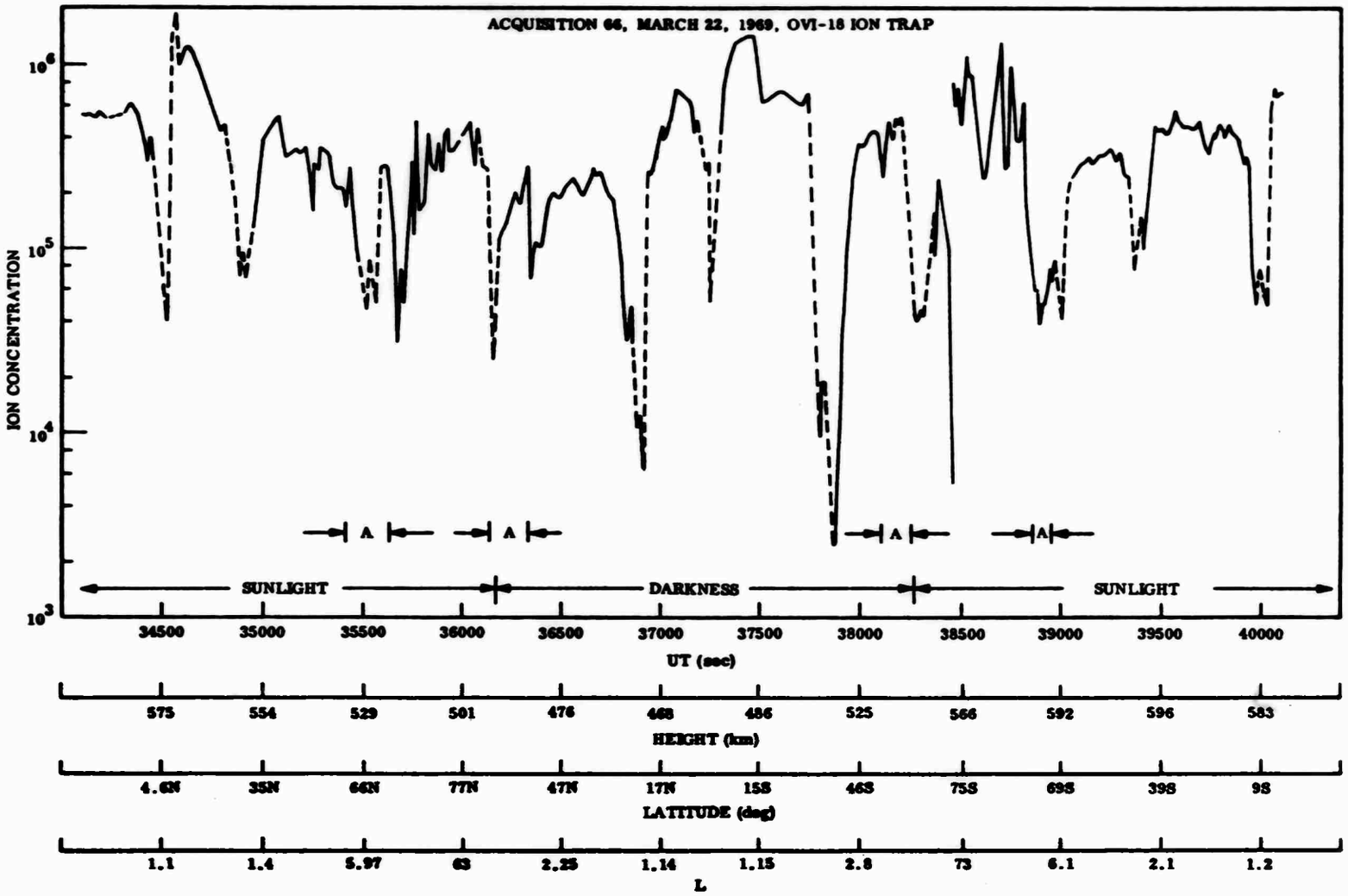

Figure 3-1 Ion Concentration from OVI-18 Ion Energy Analyzer Taken March 22, 1969, Near 1000 UT

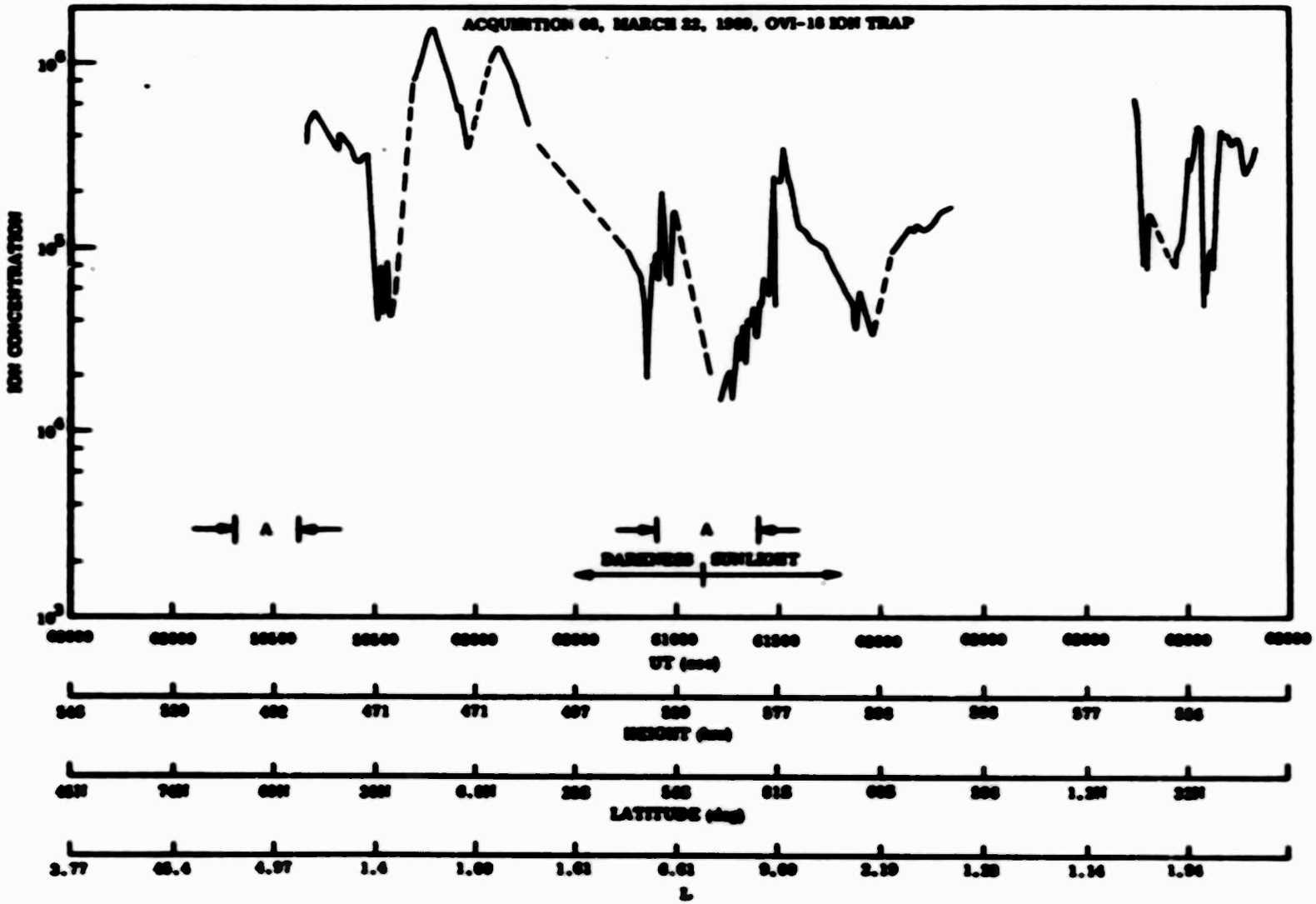

Figure 3-2 Ion Concentration from OVI-18 Ion Energy Analyzer Taken March 22, 1969, Near 1700 UT

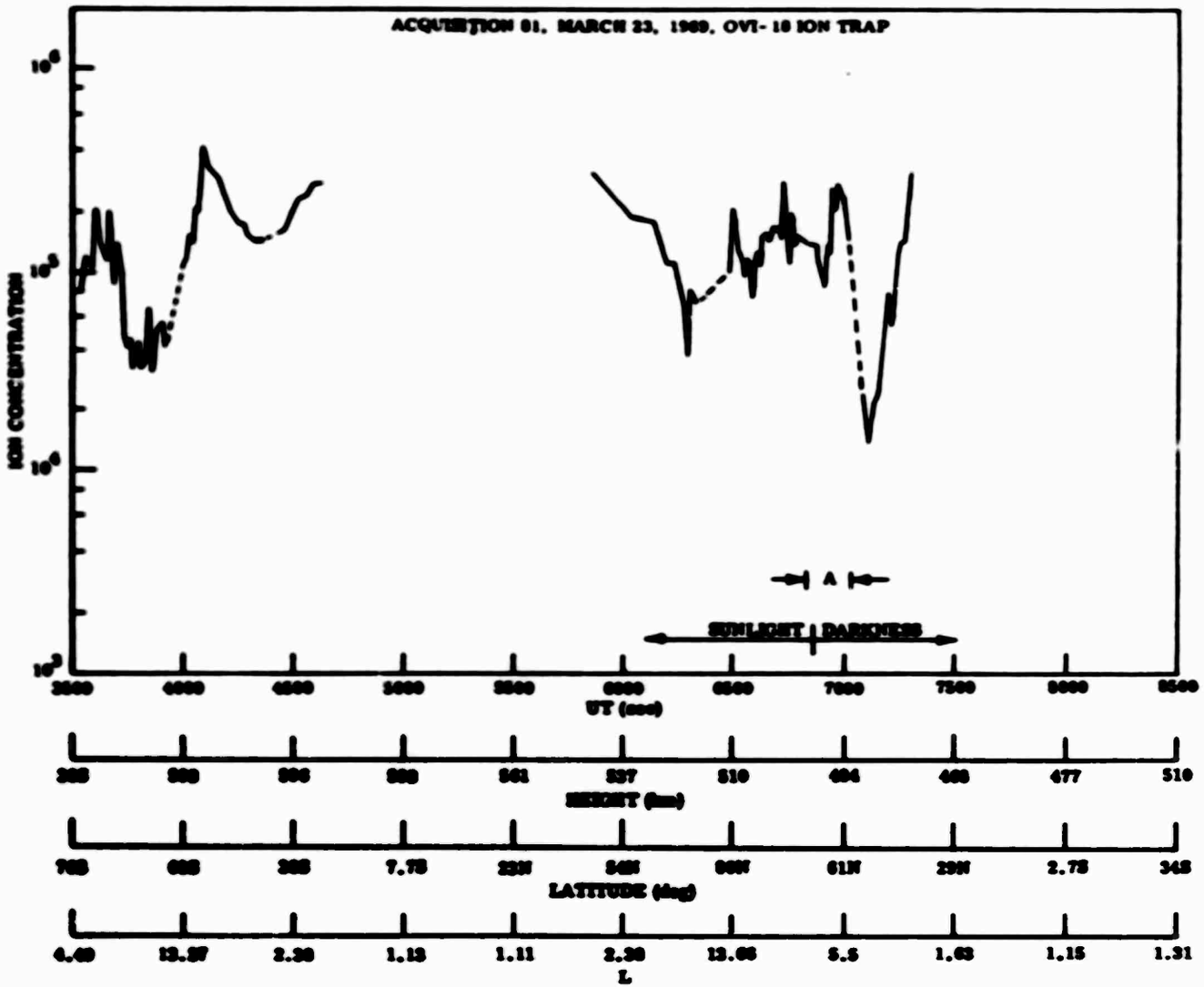

Figure 3-3 Ion Concentration from OVI-18 Ion Energy Analyzer Taken March 23, 1969, Near 0130 UT

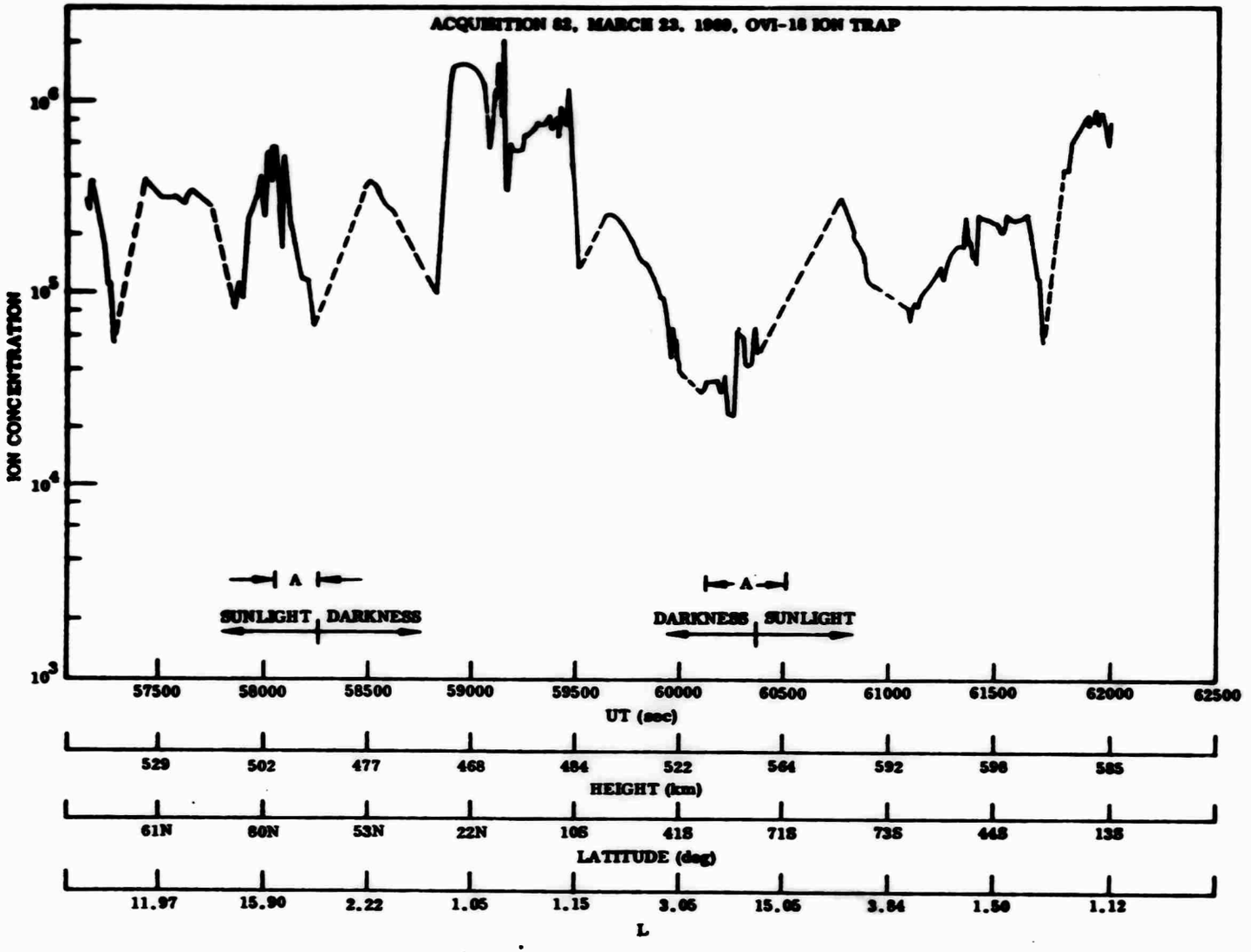

Figure 3-4 Ion Concentration from OVI-18 Ion Energy Analyzer Taken March 23, 1969, Near 1630 UT

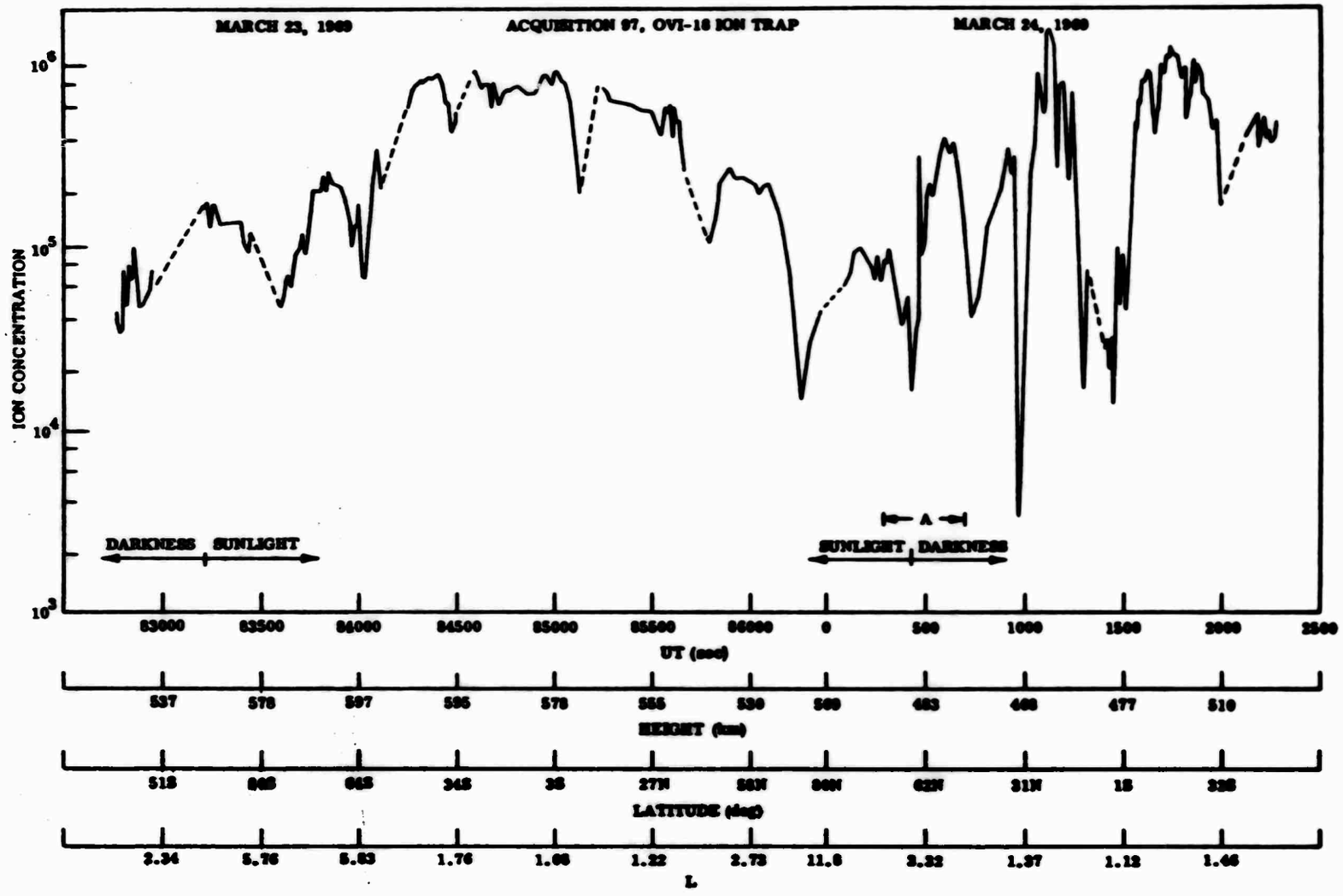

Figure 3-5 Ion Concentration from OVI-18 Ion Energy Analyzer Taken March 23, 1969, Near 2400 UT

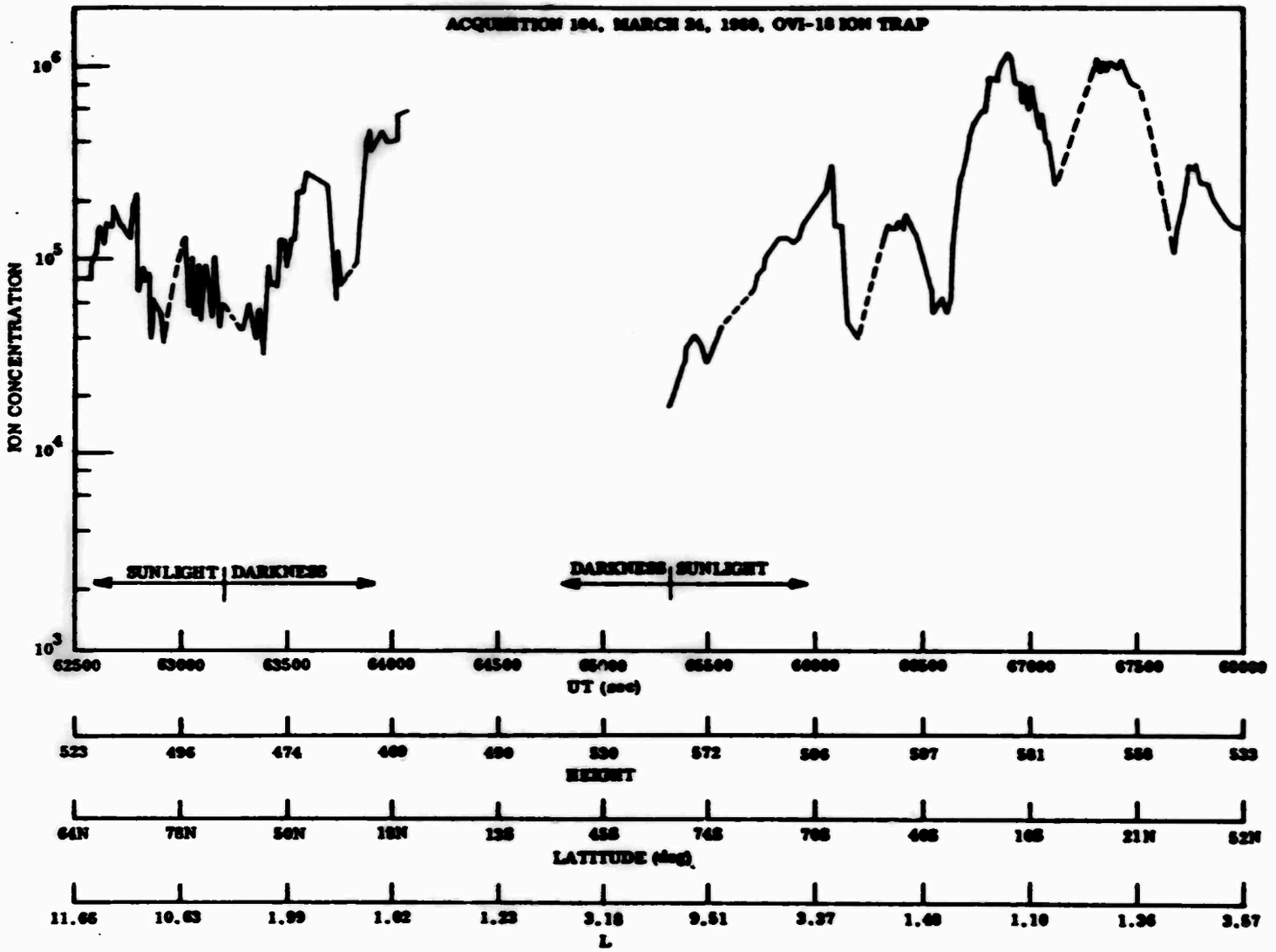

Figure 3-6 Ion Concentration from OVI-18 Ion Energy Analyzer Taken March 24, 1969, Near 1800 UT

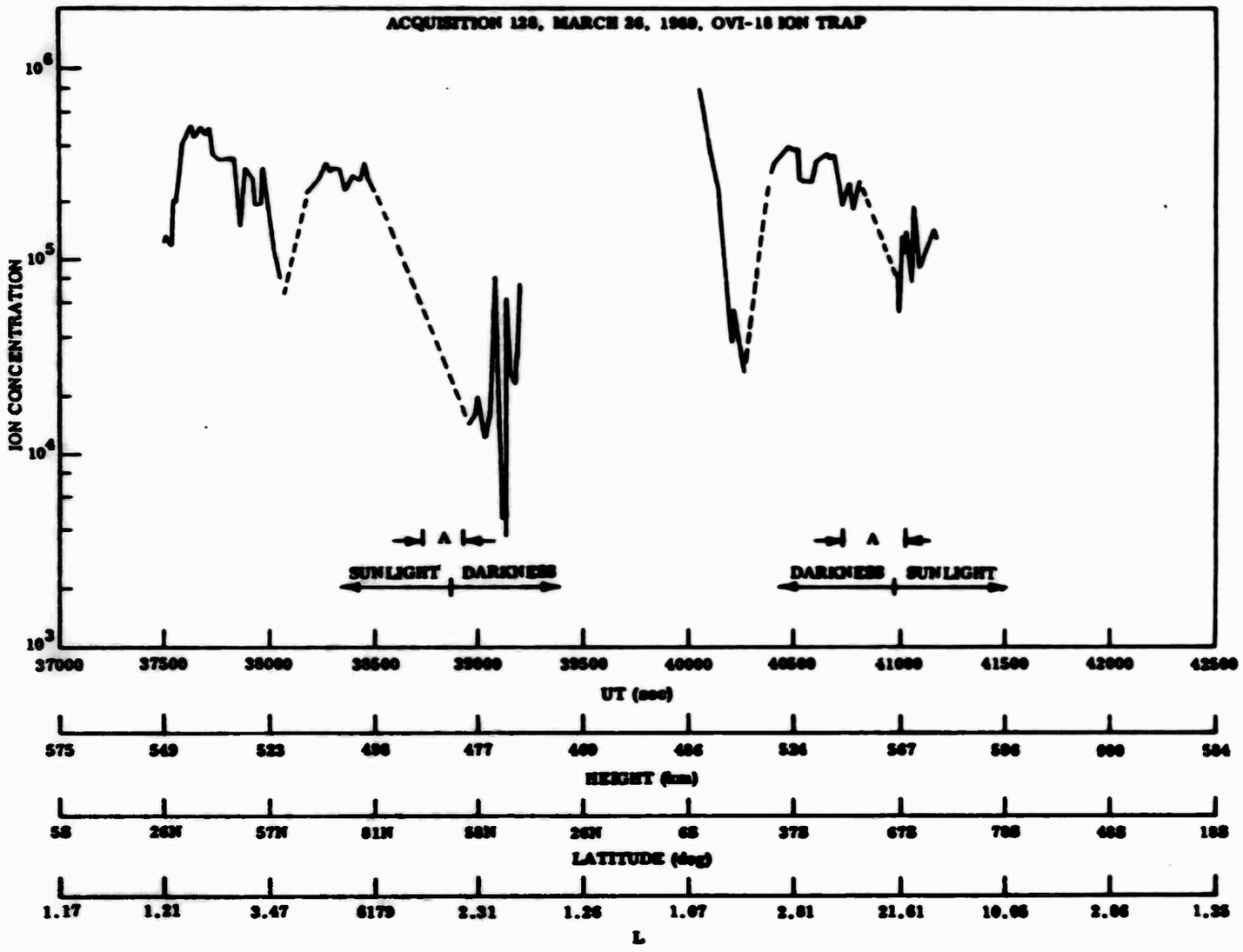

Figure 3-7 Ion Concentration from OVI-18 Ion Energy Analyzer Taken March 26, 1969, Near 1100 UT.

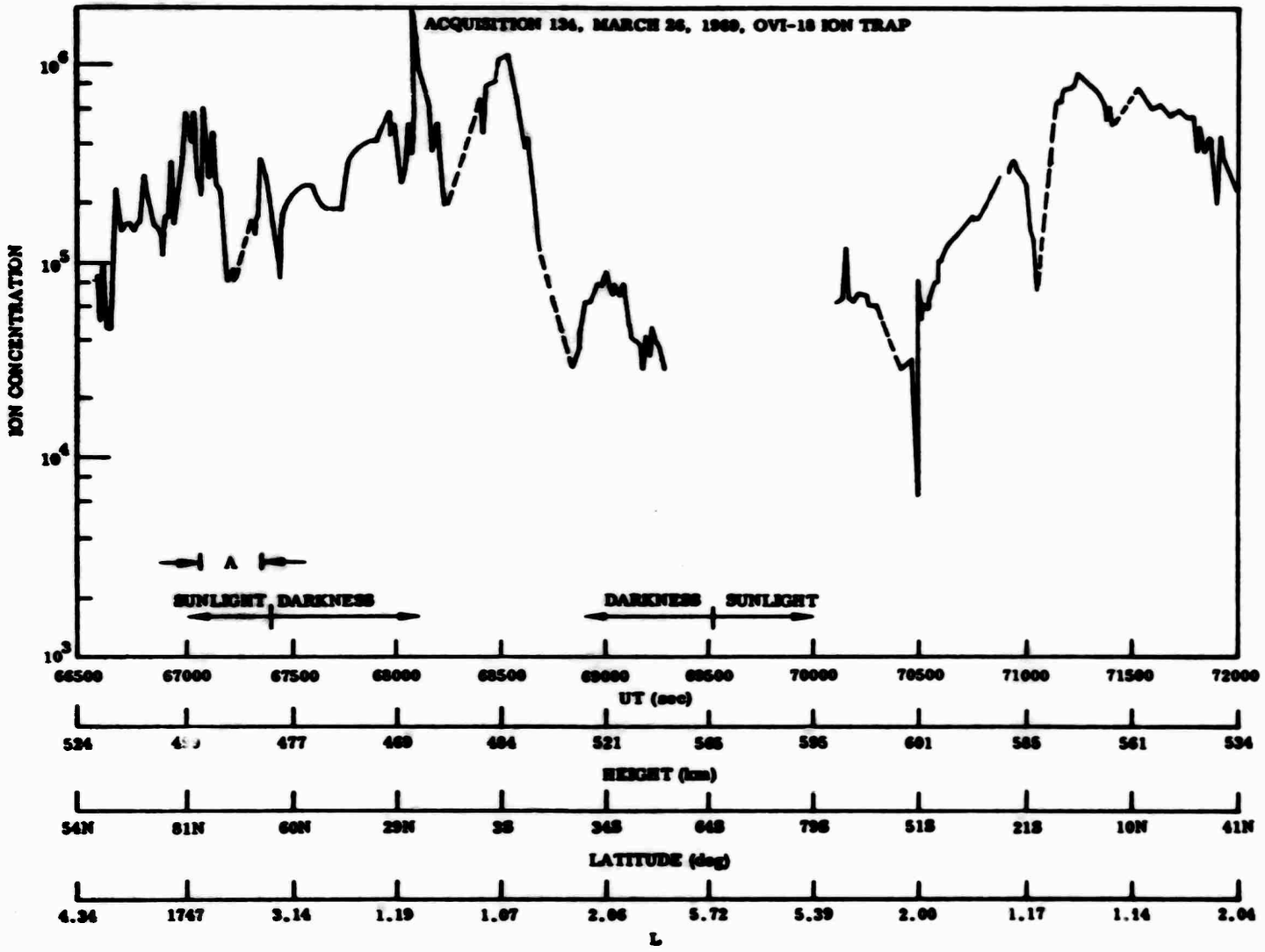

Figure 3-8 Ion Concentration from OVI-18 Ion Energy Analyzer Taken March 26, 1969, Near 1900 UT

Section 4

ELECTRON MEASUREMENTS

Section 4

Electron Measurements

4.1 Thermal Electron Density and Temperature

A cylindrical Langmuir Probe, kindly supplied by Dr. A. Nagy of the University of Michigan, was flown as a part of the ionospheric measurements package of OV1-18. The probe provides a measure of thermal electron concentration, electron temperature, and vehicle potential. The intent was to compare electron temperature (measured by this probe) with the ion temperatures to be obtained from the Ion Energy Analyzer and to evaluate the probe's usefulness as a gradient detector. A useful by-product was the vehicle potential which was needed to establish accurate energy values for the suprathermal electrons collected by the Epithermal Electron Analyzer. Unfortunately, the telemetry bandwidth available for this probe was too small to allow the probe to have the spatial resolution in its measurements to be able to do much about ionospheric gradient measurements.

Figure 4-1 is a plot of the electron concentration obtained from the Langmuir Probe for acquisition 134. As with the ion concentration plot in Figure 3-1, the electron concentration is plotted on a logarithmic scale against a linear time scale. The appropriate ephemeris information is listed on 500 second time intervals. The open circles indicate the actual data points available and point up the problem of spatial resolution. The probe makes accurate measurements of the ambient electrons except when it is in the vehicle wake. It was placed on the vehicle in such a manner that, had the vehicle been oriented, the probe would have had its axis

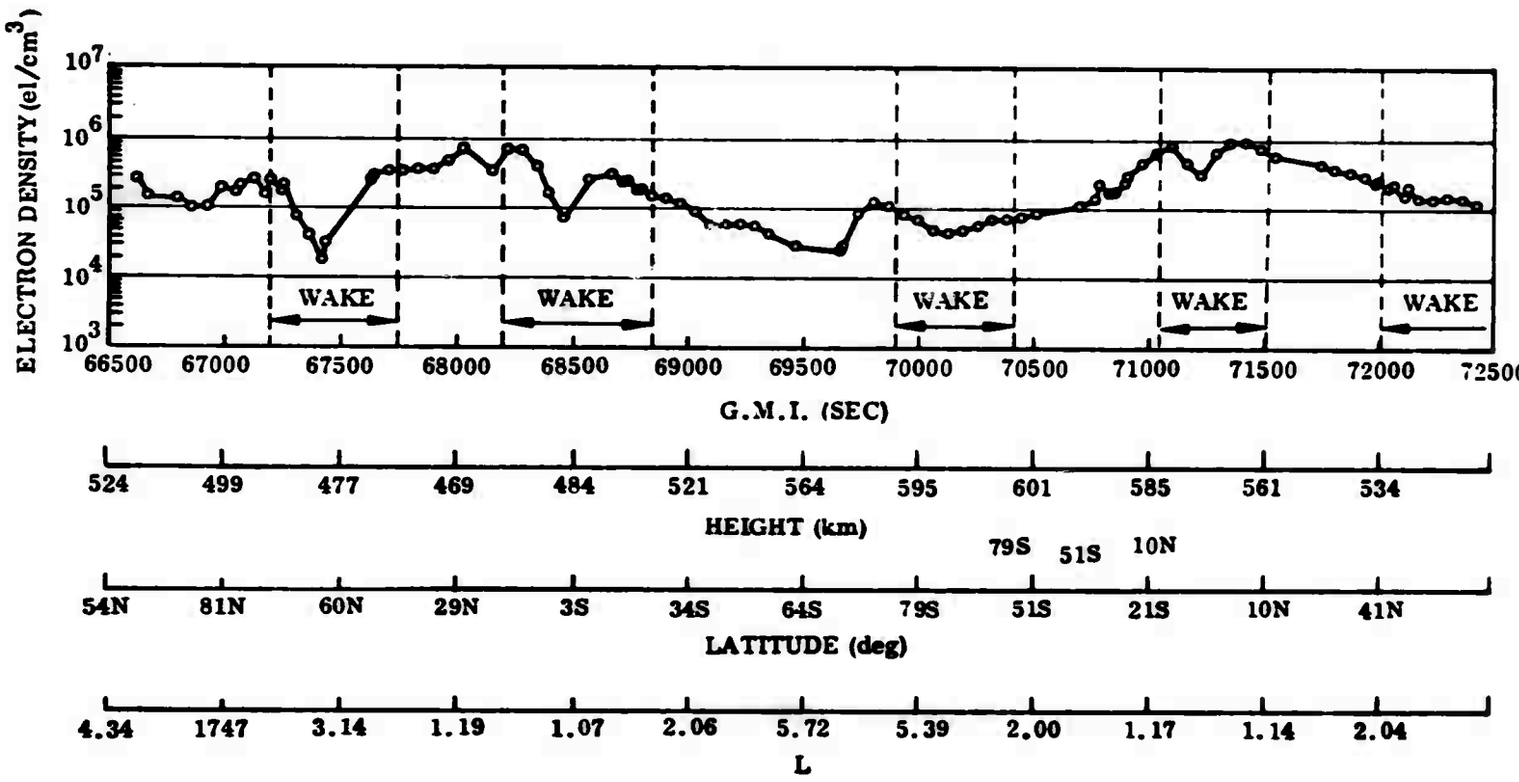

Figure 4-1 Electron Concentration from OVI-18 Langmuir Probe Taken March 24, 1969, Near 1800 UT

along the velocity vector. The spinning motion of the vehicle caused the probe to be in the vehicle wake a significant portion of the time. In Figure 4-1 the wake regions are indicated. In those regions little confidence can be placed in the data being accurate ambient electron concentration values. It should be noted, by comparing Figure 4-1 with Figure 3-8, that when the Langmuir Probe and the Ion Energy Analyzer were looking in a favorable (non-wake) direction the measured ion and electron concentrations agree very well, as they should. The IEA is able to show the structural detail that is missing from the probe data due to the poor spatial resolution provided for the probe.

All of the electron concentration data has been reduced for orbits prior to 225. However, since the data did not provide a useful input for the principle purpose of this study, a study of ion gradients, the full set of data are not shown here. The Second Quarterly Technical Report showed a plot like Figure 3-8 for acquisition 66.

The electron temperature and vehicle potential have also been derived from the data from each of these orbits prior to number 225. We will not show any vehicle potential data here as it has no specific geophysical value and does not contribute to the general objectives of this study. Figure 4-2 is a plot of the electron temperature derived from the Langmuir probe for acquisition 134. In the plot, the ambient electron temperature is plotted on a linear scale as a linear function of time and, as in Figure 4-1, appropriate ephemeris information is supplied on 500 second intervals. The wake regions are indicated to show where the data may be suspect. However, as can be seen in the figure, the electron

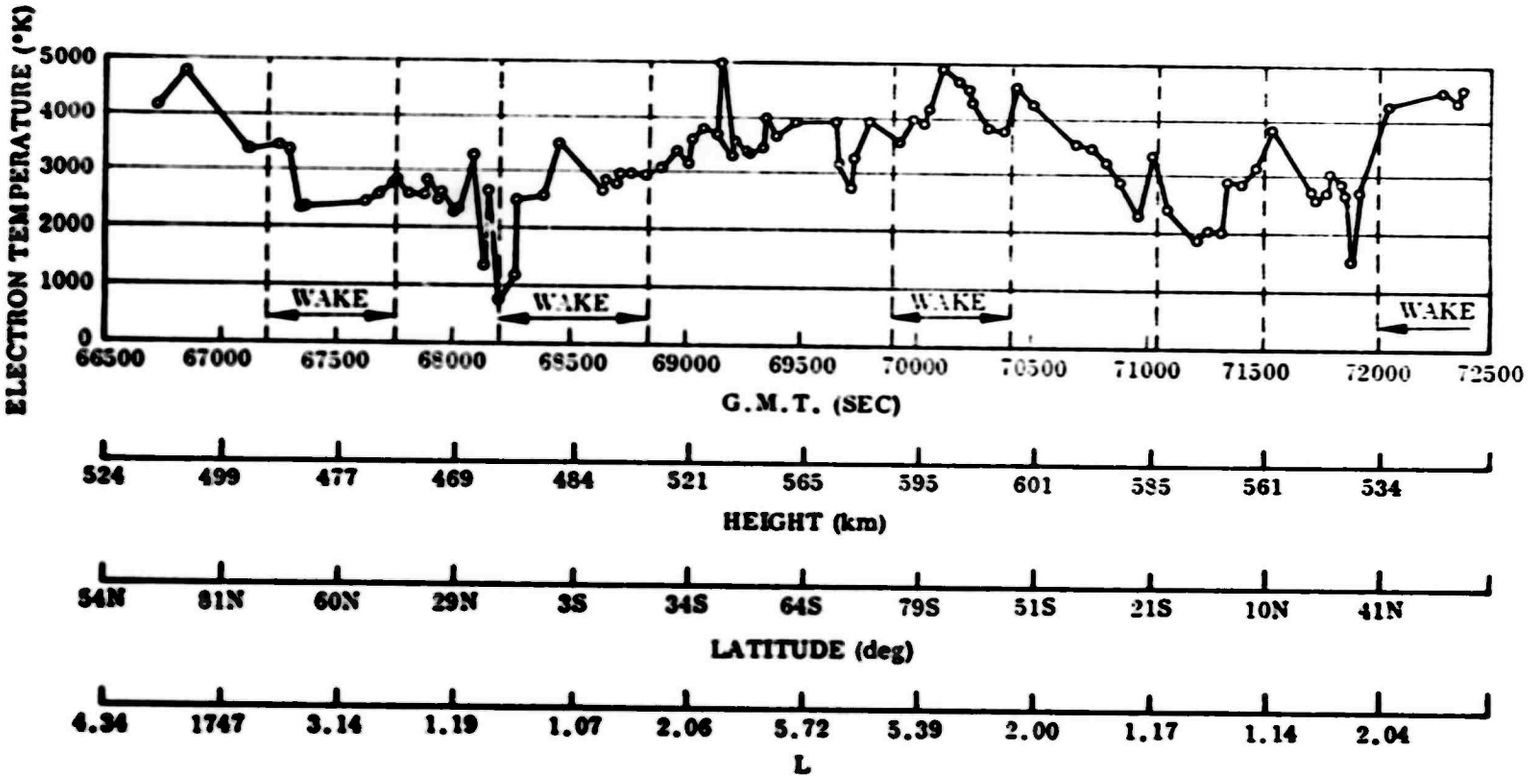

Figure 4-2 Electron Temperature from OVI-18 Langmuir Probe Taken March 24, 1969, Near 1800 UT

temperature curve seems to flow smoothly through the wake regions, from non-wake to non-wake region, which gives support to the idea that even the wake-measured temperatures may be valid temperature measurements. Observe that the electron temperatures measured in the high latitude regions are 1000° to 1500°K higher than those measured in the low latitude regions. Poor spatial resolution does not permit detailed comparison of the data to possible high latitude energy sources.

4.2 Epithermal Electrons

Figures 4-3, 4-4, and 4-5 show the fluxes of electrons in each of 6 energy channels measured by heads 1, 2, and 3 of the Epithermal Electron Energy Analyzer (EEA) experiment for acquisition 66. In the figures the flux is plotted on a logarithmic scale with the scale for each decreasing channel number displaced downward by one decade.

Fluxes in a seventh, highest energy channel (3) have been measured also but not illustrated. The energy interval corresponding to each channel and the factor by which fluxes in each channel must be multiplied to obtain fluxes in units of cm^{-2} sec^{-1} $ster^{-1}$ ev^{-1} are given in Table 4.1. To each energy listed must be added the vehicle potential value to give the actual electron energy.

The following general observations are readily evident:

The fluxes in the more energetic channels 7-3 are drastically reduced at night where photo production of electrons is essentially absent. Exceptions to this generalization occur in the nightside auroral zones where the fluxes in all channels are about equal and at low invariant L latitudes of 1.1 and 1.7 where relatively large fluxes of electrons (or negative ions) were observed in channel 7 as well as in 8 and 9.

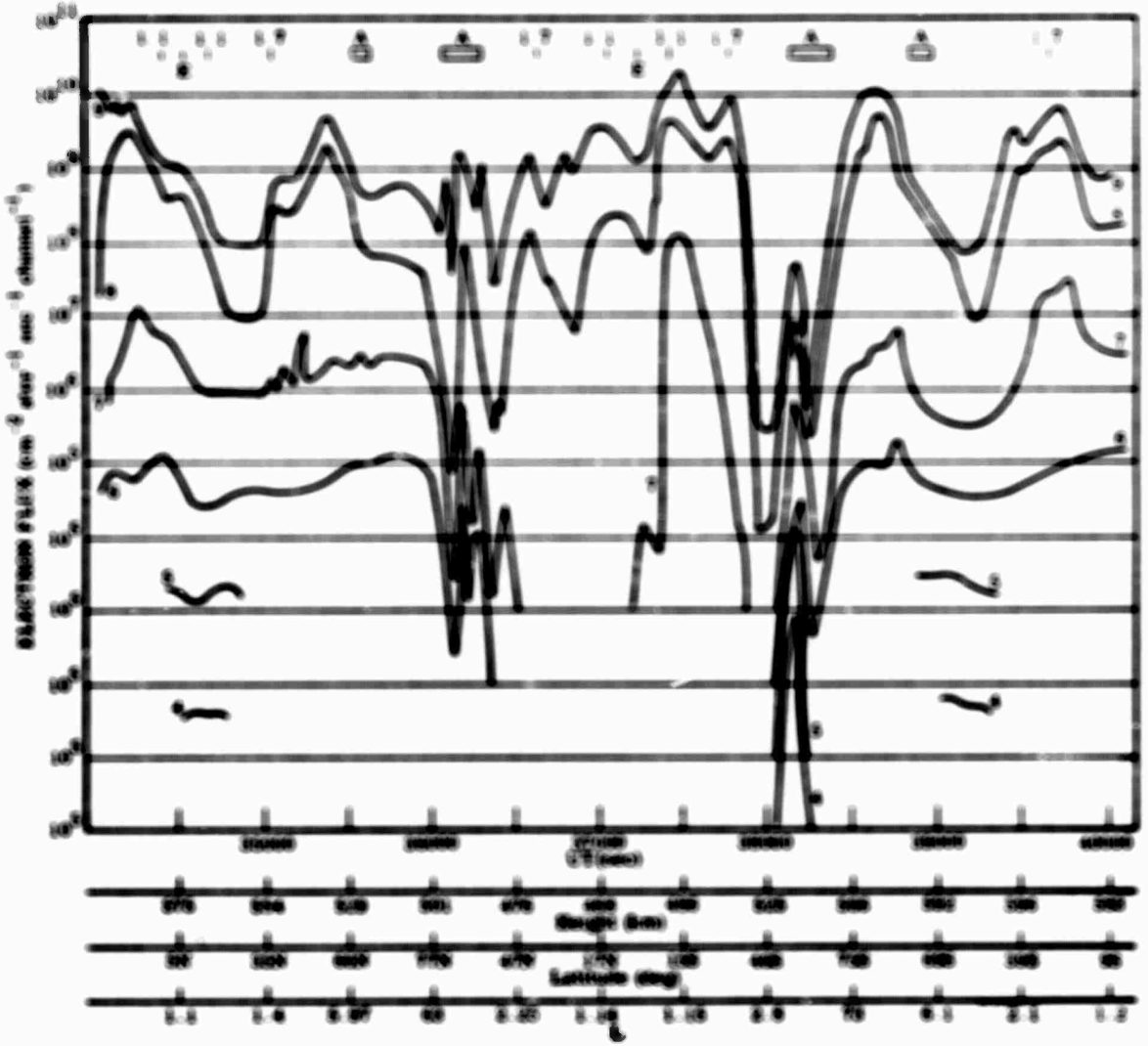

Figure 4-3 Suprathermal Electron Flux from OVI-18 Epithermal Electron Analyzer, Read No. 1, taken March 22, 1969.

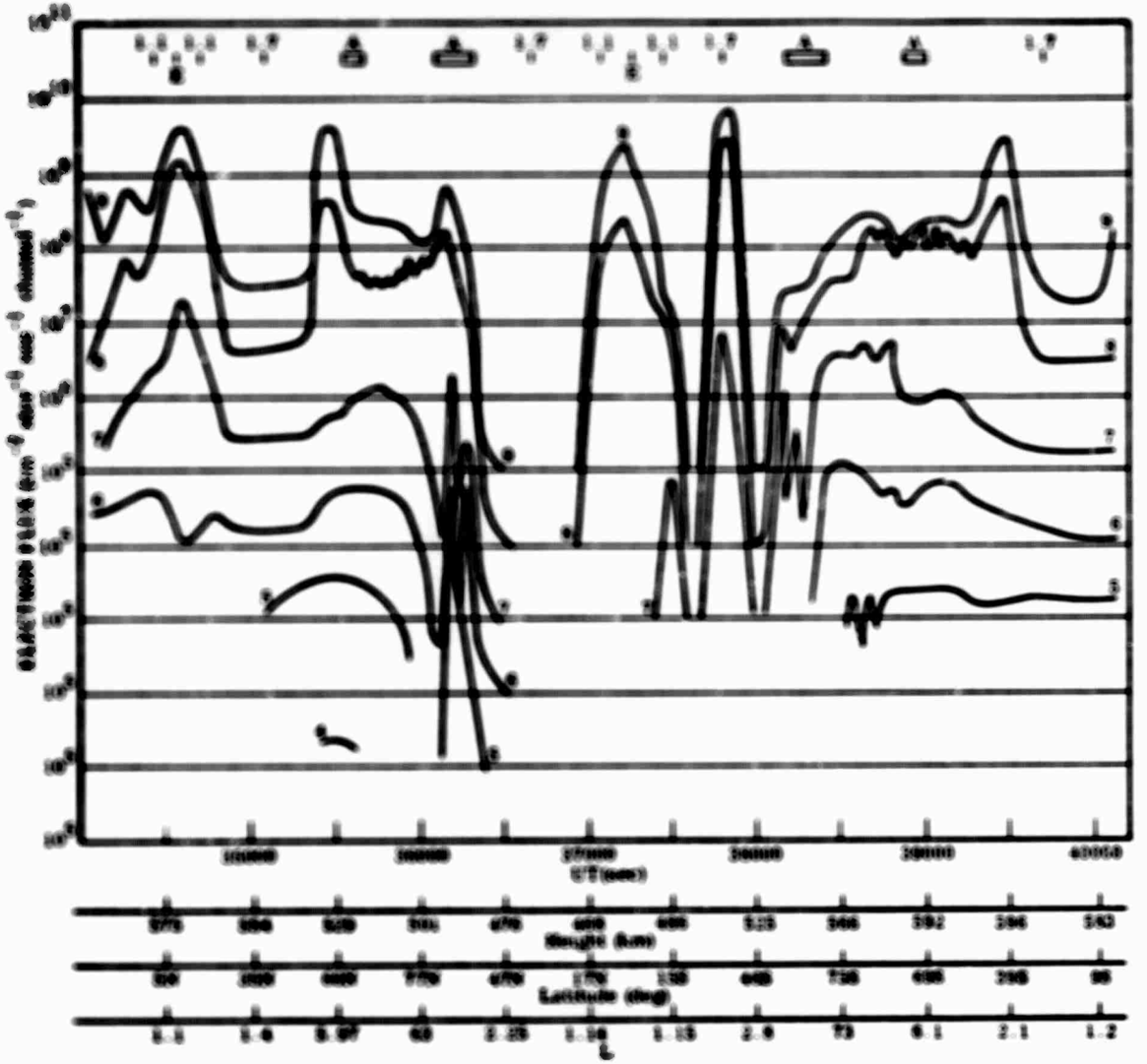

Figure 4-4 Suprathermal Electron Flux from OVI-18 EEA, Head No. 2, taken March 22, 1969.

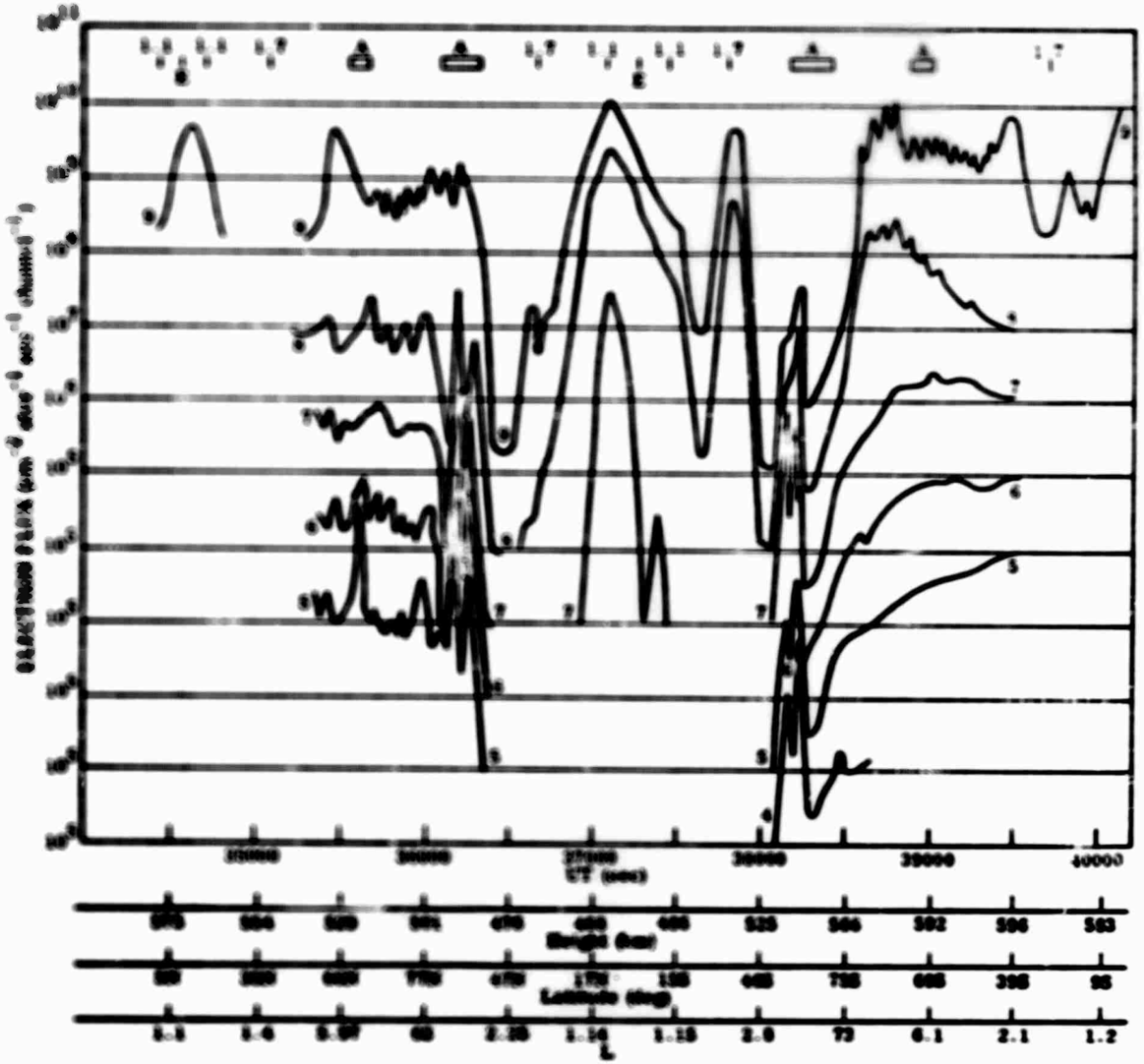

Figure 4-5 Suprathermal Electron Flux from OVI-18 EEA, Reel No. 3, taken March 22, 1969.

Table 4.1

EEA Channel Conversion Factors

Channel	Energy Interval (eV) *	Conversion Factor Channel eV^{-1} **
9	0 - 2	0.465
8	2 - 4	0.593
7	4 - 8	0.297
6	8 - 16	0.149
5	16 - 32	0.074
4	32 - 64	0.037
3	64 - 128	0.019

* This energy is measured relative to the potential energy of the vehicle which was typically 3-4 eV.

** The fluxes given in Figures 4-3, 4-4, and 4-5 when multiplied by this factor became fluxes in units of cm^{-2} sec^{-1} $ster^{-1}$ eV^{-1} centered at the energy approximately equal to the upper value specified in the Energy Interval column.

(Missing data on all channels during daylight results when the particular head is oriented toward the sun.) Note that the auroral regions are indicated in the figures by enclosed rectangles above the data.

The fluxes observed at night in channels 7, 8 and 9 by the three separate heads were different by several orders of magnitude at times. Some of the difference may be caused by wake effects which have been documented by Samir and Wilmore (1965). The difference could also result from anisotropy of the electron flux or from the electron energy analyzer scooping up negative ions.

A substantial fraction of the time--both day and night--the flux in channel 8 was larger than channel 9. This means that there was a relative maximum in the flux vs. energy spectrum at an energy of about 7 eV (since the vehicle potential was measured to be -3 Volts at these times). Such a hump has been predicted at lower altitude and during daylight by theoretical studies (Nagy and Banks, 1970; Dalgarno et al., 1969) but has not been expected at night. A large fractional content of O^- ions in the ionosphere would produce the same effect.

Evidence for enhanced flux in all channels over the magnetic polar cap regions (tail field lines) is present in the figures, but that the enhancement is caused by energetic electrons from the magnetic tail and not by an unanticipated solar effect needs to be investigated.

References

Dalgarno, A., M. B. McElroy, and A. I. Stewart, "Electron Impact Excitation of the Dayglow," J. Atmos. Sci., 26, 753, 1969.

Nagy, A. F. and P. M. Banks, "Photoelectron Fluxes in the Ionosphere," J. Geophys. Res., 75, 6260, 1970.

Samir, U. and A. P. Wilmore, "The Distribution of Charged Particles Near a Moving Spacecraft," Planet. Space Sci., 13, 285, 1965.

Section 5

ENERGETIC PARTICLES

Section 5

ENERGETIC PARTICLES

The principal information on the low-energy auroral particle fluxes has been derived from two types of detectors, one for the electron measurements and one for the proton measurements. Both types use channel electron multipliers as the sensing elements. The CME detectors are individual 180° permanent magnet spectrometers used for the electron measurements. They are designed with broad, flat, response functions and are arranged contiguously so that they cover the energy range of interest without leaving gaps. A group of such spectrometers is oriented in each of three directions, referred to as the 0° detectors (Group 1), the 55° detectors (Groups 2 and 3) and the 90° detectors (Group 4). The characteristics of the individual units are listed in Table 5.1. The proton detectors, referred to as CFP's, use magnetic brooms to sweep out the electrons, and thin carbon or nickel foils to define the thresholds to incident protons. The characteristics of these detectors are also listed in Table 5.1.

The responses of some of these detectors for the nightside traversals of the northern and southern auroral zones on March 22, 1969 are illustrated in Figure 5-1. Each trace is the output of a logarithmic rateneter which compresses about four decades of dynamic range into the illustrated intervals. The pitch angle appropriate to the Group 1 detectors is shown in the top curve (180° corresponds to a flux coming down the field lines). The CMEIC detector was experiencing a temporary malfunction during part of the period illustrated and its output has been replaced in the plots and subsequent calculations by that of CME3C. The first double peak in the northern hemisphere polar cap region is an in-flight calibration. As the satellite moves southward into the auroral zone it encounters a highly structured flux of soft electrons, which rapidly hardens as the satellite approaches the lower latitudes. A broad double-peaked region of proton precipitation is

Table 5.1

Detector Characteristics

Detector Name	Type of Particle Analyzed	Energy Range (keV)	Geometric Factor (cm^2 - sr)	Nominal Pointing Direction (deg)
CME1A	e^-	0.80 - 1.50	8.70×10^{-6}	0
1B	e^-	1.75 - 3.30	8.10×10^{-6}	0
1C	e^-	3.75 - 7.00	9.60×10^{-6}	0
1D	e^-	8.30 - 16.3	2.56×10^{-5}	0
1E	e^-	17.30 - 37.0	4.04×10^{-5}	0
1F	e^-	Background	---	0
CPP1B	p^+	> 9.0	1.30×10^{-4}	0
1D	p^+	> 38.	1.30×10^{-4}	0
CME2A	e^-	0.80 - 1.50	7.45×10^{-6}	55
2D	e^-	8.20 - 16.5	2.24×10^{-5}	55
CPP2A	p^+	> 5.0	3.25×10^{-5}	55
2C	p^+	> 24.	1.30×10^{-4}	55
2E	p^+	> 6500.	1.30×10^{-4}	55
CME3B	e^-	1.80 - 3.30	8.45×10^{-6}	55
3C	e^-	3.75 - 7.00	9.80×10^{-6}	55
CPP3B	p^+	> 7.7	3.25×10^{-5}	55
3D	p^+	> 38.	1.30×10^{-4}	55
CME4A	e^-	0.80 - 1.50	7.60×10^{-6}	90
4B	e^-	1.80 - 3.25	9.40×10^{-6}	90
4C	e^-	3.70 - 7.00	8.50×10^{-6}	90
4D	e^-	8.40 - 16.3	2.49×10^{-5}	90
CPP4B	p^+	> 14.	6.50×10^{-5}	90
4D	p^+	> 38.	6.50×10^{-5}	90

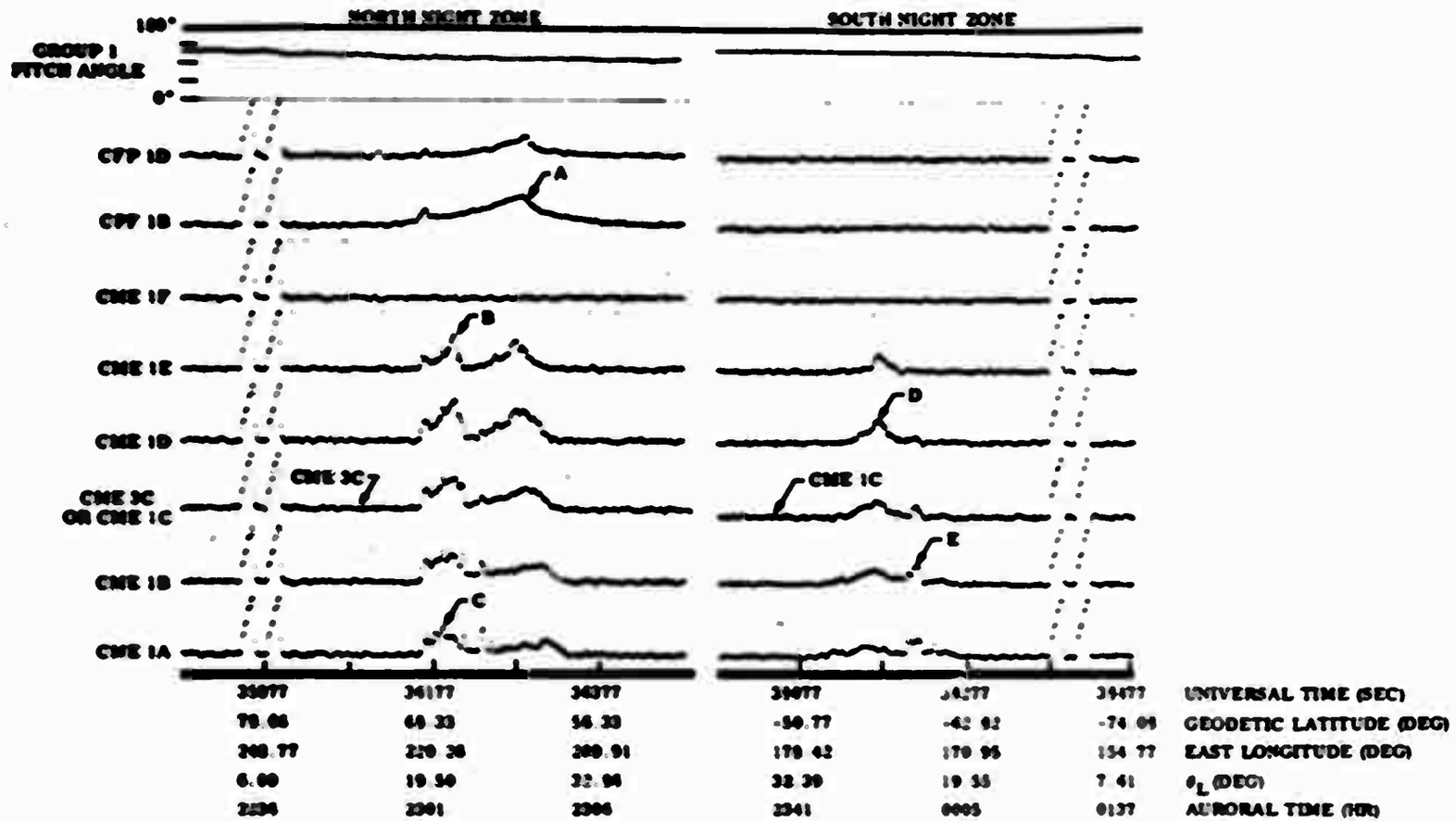

Figure 5-1 Precipitated Electrons and Protons from the OVI-15 CME Detector and CPP Detectors taken in the North Night Zone and the South Night Zone, March 22, 1969.

also encountered. A similar sequence is illustrated for the southern hemisphere auroral zone traversal in this figure except in this case no protons were observed. The typical high-latitude spectral softening of the electrons is clearly evident.

Table 5.2 shows some typical flux characteristics derived from these measurements at the times indicated by the letters in Figure 5-1. For the electrons the flux shown is the integral number flux of electrons with E ≥ 10.3 keV and E_o represents the flux weighted average energy. For the protons the flux is the integral number flux of protons with E ≥ 9 keV and E_o represents the characteristic or average energy of an assumed exponential spectral shape fitted to the results from the two threshold detectors.

Table 5.2

Flux Characteristics

Point	Universal Time (sec)	Type of Particles	Number Flux (Particles/ cm^2-sec-sr)	E_o (keV)	Pitch Angle (deg)
A	36284	p^+	6.74×10^6	20.6	94
B	36203	e^-	3.14×10^8	7.76	99
C	36189	e^-	3.38×10^8	5.44	98
D	38168	e^-	3.31×10^7	6.91	124
E	38216	e^-	5.32×10^7	2.44	125

The period of primary interest for the intercomparison of the ionospheric and particle measurements, i.e., the first 225 orbits, was a period of highly variable auroral activity. It included two extremely "quiet" days (designated QQ in the tables of Solar-Geophysical Data) and four "disturbed" days, including a prominent magnetic storm on 23 and 24 March. The magnetic activity index Ap for the period of interest is plotted in Figure 5-2. The data in Figure 5-3(A97) were obtained on March 24 during the storm period and the data in Figure 5-4(A144) were obtained during the

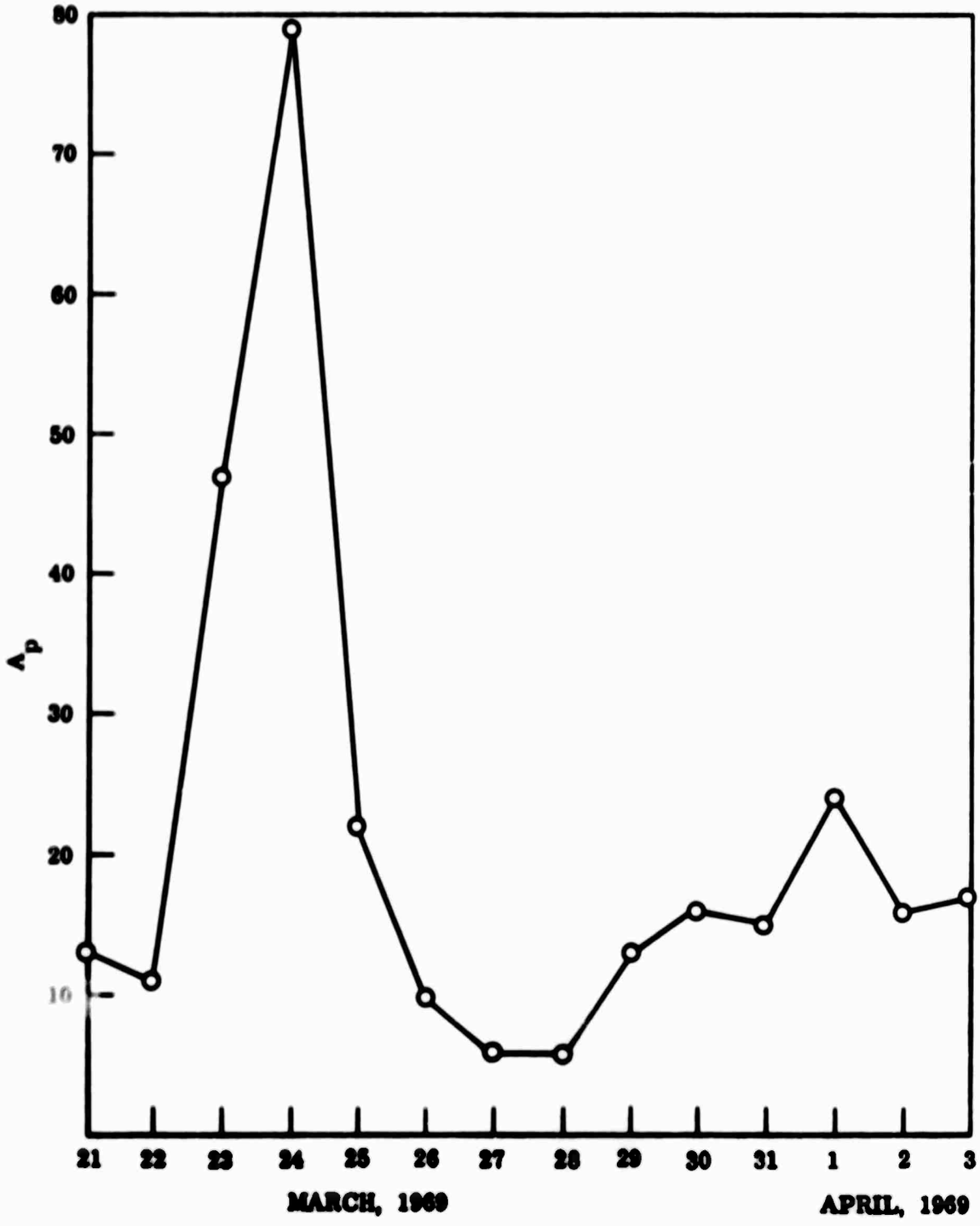

Figure 5-2. Magnetic Activity During First 225 Revolutions

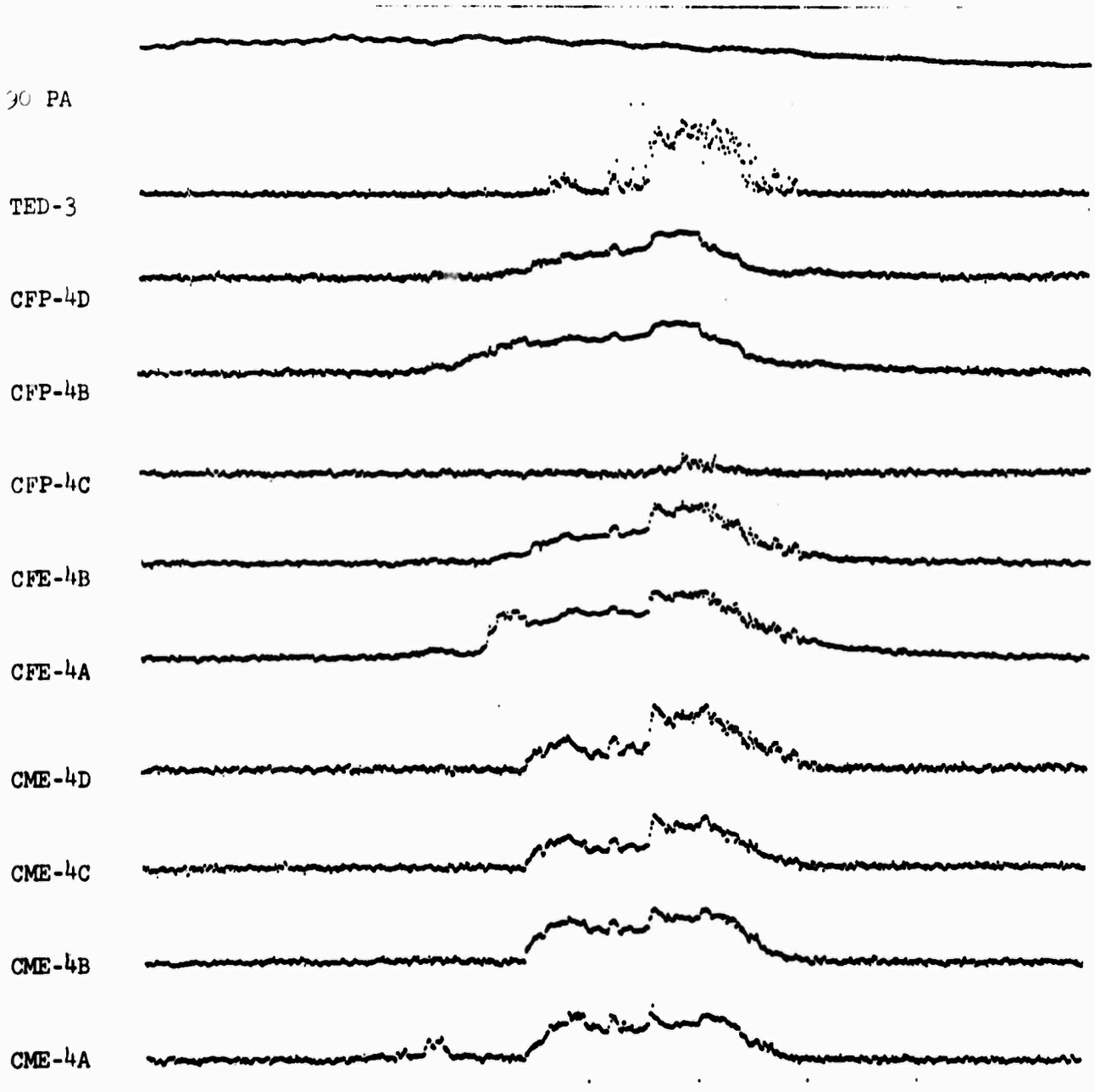

UT (SECONDS)	171	271	371	471	571	671	771	871
INVARIANT CO-LATITUDE (DEG)	15.4	17.9	21.9	26.7	32.1	37.7	43.7	50.2

Figure 5-3. A97, 24 March 1969

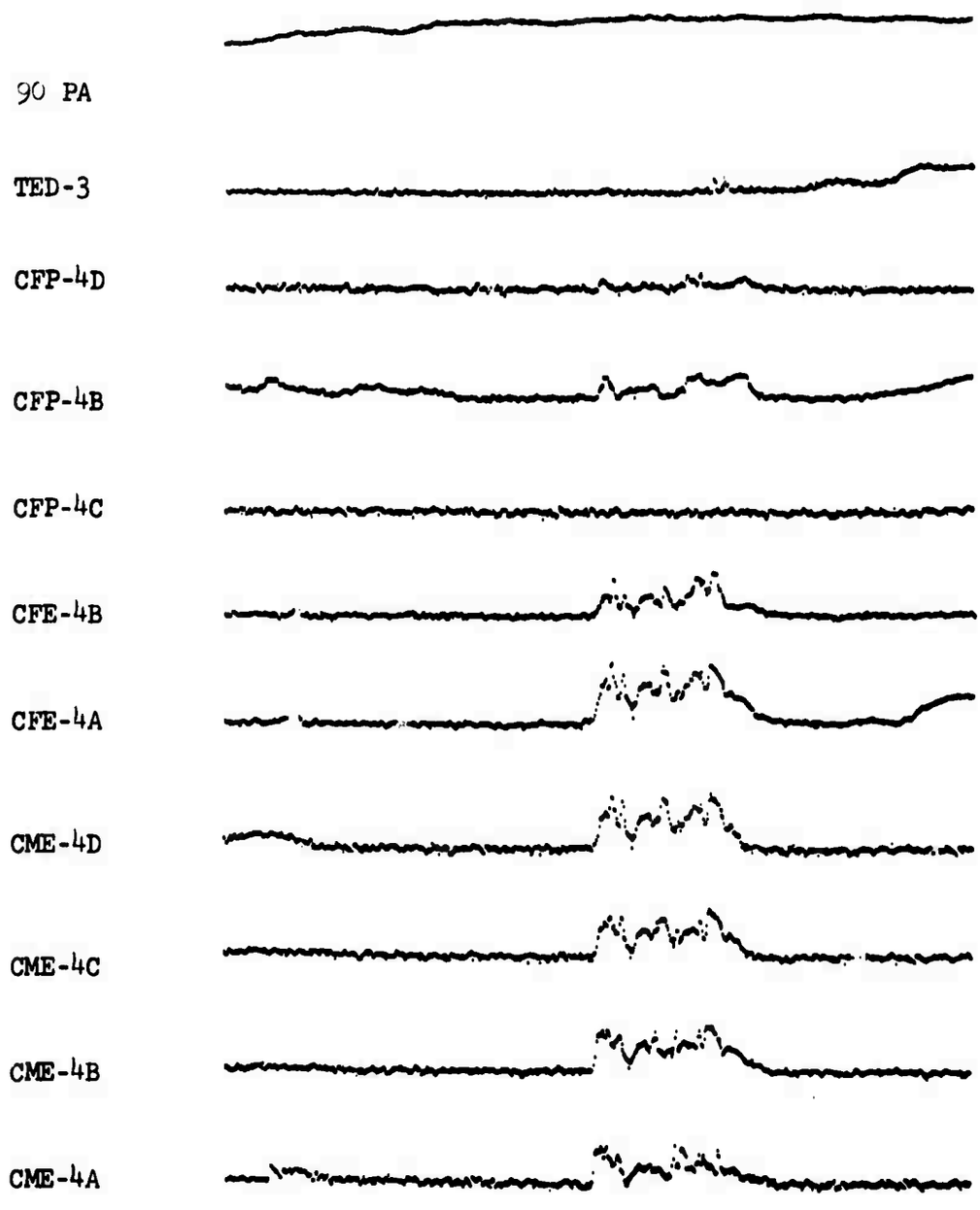

UT (SECONDS)	37774	37874	37974	38074	38174	38274
INVARIANT COLATITUDE (DEGREES)	2.3	8.9	15.7	22.5	29.3	35.8

Figure 5-4. A144, 27 March 1969

quiet day of 27 March. As seen in the figures, a substantial difference in the general level of auroral activity is evidenced between the two days, and the location of the precipitation region has shifted significantly in magnetic latitude.

Section 6

ION GRADIENT/PARTICLE COMPARISONS

Section 6

Ion Gradient/Particle Comparisons

6.1 Ion Gradients

In Section 3 we discussed the general character of the ion concentration data that was obtained from the OV1-18 vehicle and figures were shown depicting this data for eight acquisitions of the satellite. Since there are a rather large number of steep gradients in the ion concentration plots shown there, it would seem appropriate to discuss these here. We will consider in detail acquisition 66, shown in Figure 3-1, since it seems to be typical. This data was taken during a period of rather high magnetic activity. It can be seen that a number of the large gradients contain significant portions that are dashed, therefore their validity may be in question. The first one, just prior to 34500 sec. is a trough which may well be completely suspect. However, the second trough, at about 34800 sec., must be real, although its exact shape may be different than that shown. On the basis of this suspect data only the troughs at 34500 sec., 36100 sec., 37200 sec., and 38250 sec. could be largely eliminated or really drastically reduced. The other troughs have enough good data to establish at least one wall, as indicated by the solid portion of the curve.

The auroral zone shown at 35500 sec. is the North day zone and the one at 36300 sec. is the North night zone. Between these two zones the spacecraft is traveling through the Polar Cap region and the ion concentration shows a lot of sharp structure as would be expected. However, the total ion concentration is higher in both this and the southern polar

cap (38500 - 39000 sec.) than is usually seen at this altitude. Since this was a disturbed period of time, the increased ionization in the polar caps is to be expected. The so-called "mid-latitude" troughs appear just equatorward of the night auroral zones (36800 sec. and 38000 sec.) but are not particularly prominant features in Figure 3-1. These will be discussed in greater detail later.

The rather deep troughs at about 36900 sec. and 37800 sec. are unusual features of the data. No explanation is available for their existence although similar things have been observed at night on other satellite flights. Their existence does seem to be real, however. In comparing this data to that obtained from other satellite flights, the most stratling feature is the large amount of structure seen in the daytime ionosphere. Normally the solar photoionization completely dominates the dayside ionosphere with a relatively smoothly varying distribution of ionization with latitude. It may be that the high magnetic activity during this pass can account for this structure in some way.

Examination of the dashed portions of the curves in the other seven ion concentration plots in Section 3 reveal that most of the gradients must really exist because they are established by one wall of really reliable data. A further test of the validity of the troughs and gradients seen on the individual plots is a comparison of these features on different acquisitions. Experience has shown that most latitudinal features of the ionosphere are controlled by the earth's geomagnetic field. This is to be expected since charged particles can move rather freely along magnetic field lines but require significant application of force to move them across field lines.

The most effective way to make this orbit to orbit comparison, then, would be to plot the data as a function of magnetic latitude. It has not been convenient to do that at this point with the data. However, an approximation to that has been performed to enable a comparison of data from two different acquisition, 66 and 97, and is shown in Figure 6-1. This figure consists of a portion of the data shown in Figure 3-1 (acquisition 66) geomagnetically aligned with a corresponding portion of the data shown in Figure 3-5 (acquisition 97). Each curve is plotted as a function of Universal Time but the Magnetic Latitude is shown on 500 second intervals. The magnetic alignment of the two curves was done using a mid-latitude magnetic reference point and the alignment is probably best at middle and low latitudes.

Even with this somewhat crude alignment procedure, common gradient features line up quite well as are indicated by the four double-headed arrows shown in Figure 6-1. Even other gradients in the upper curve appear to have some relationship to gradients in the lower curve. They do not appear to be as well aligned as the four marked by the arrows, but perhaps with careful plotting of the data against magnetic latitude these differences would be resolved. In any event, the data seen in Figure 6-1 does provide a validity proof that the observed gradients seen from OVI-18 are real gradients and are not generated by the rather erratic motion of the spacecraft.

6.2 Gradient/Particle Comparisons

One of the main objectives of this Ion Gradient program was to evaluate the mechanisms for creation of horizontal gradients, and in particular, to study the role that precipitated energetic particles may play.

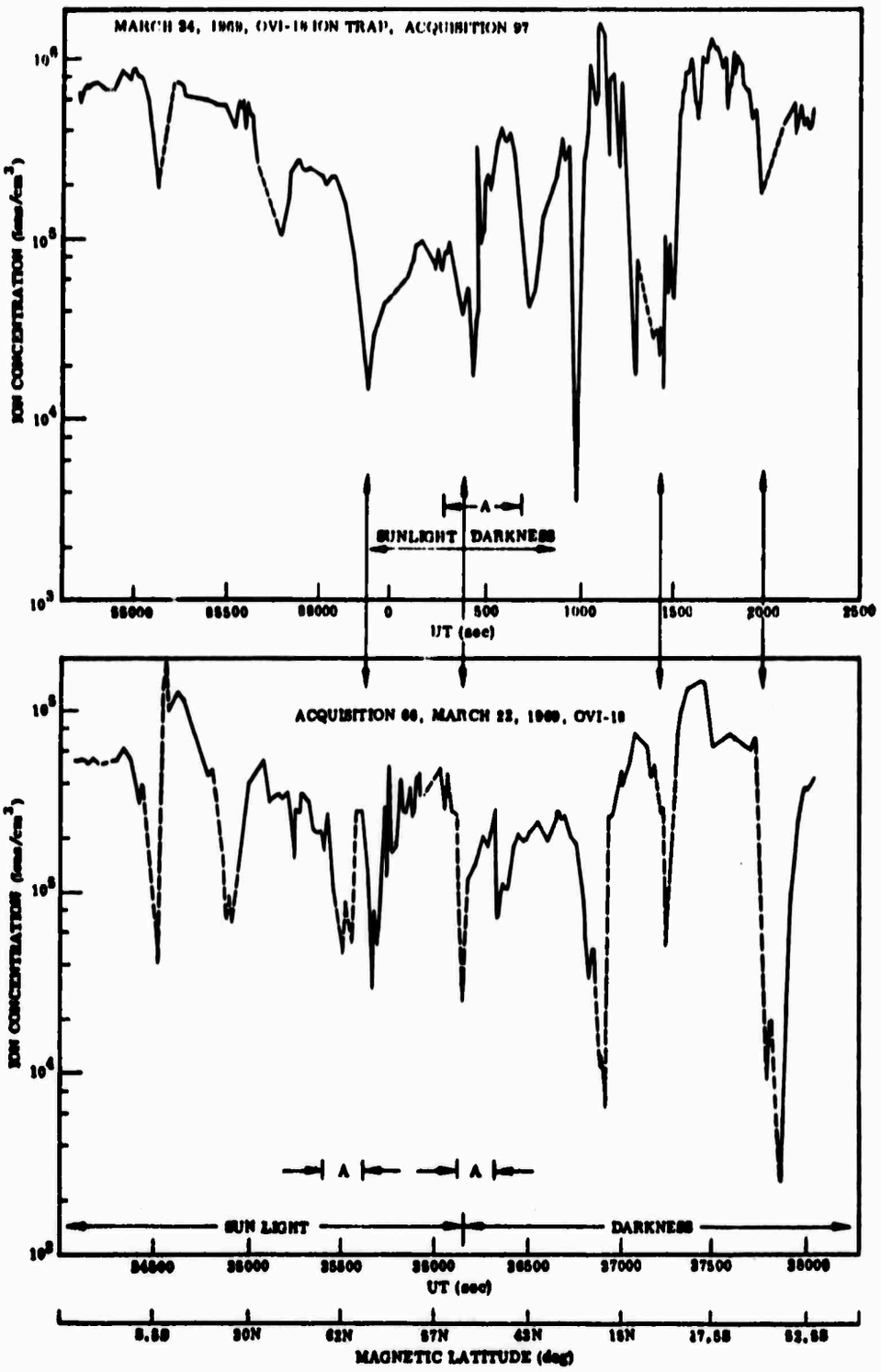

Figure 6-1 Comparison, by Geomagnetic Alignment, of Certain Ion Concentration Gradients Seen in Acquisition 66 and 97

The upper portion of Figure 6-2 shows the ion concentration data through the night northern auroral zone from acquisition 66 of OVI-18. For reference, this portion of data is taken near the second (from the left) "A" region in Figure 3-1. In Figure 6-2, however, the ion concentration is plotted on a linear scale. In the lower part of this figure is a plot of the integrated precipitated electron flux in the 1 to 37 keV energy range. This data is obtained by summing the flux measured by the CME1A, CME1B, CME3C, CME1D, and CME1E detectors and is plotted on a logarithmic scale as a linear function of time. The ion concentration and the precipitated flux are plotted against the same time scale and on this scale, at 100 sec. intervals, are shown the pertinent ephemeris information.

At 36,000 sec. the vehicle is in the polar cap region; and as can be seen from Figure 3-1, the vehicle is still in the sunlight. The relatively low ion concentration values between 36,100 and 36,200 sec. are typical for the polar cap region. Between 36,170 and 36,345 sec. the auroral zone particles are observed. Their effect upon the ionosphere is shown by increased ion density between 36,200 and 36,335 sec. The so-called "mid-latitude trough" of the night ionosphere is seen between 36,335 and 36,400 sec. The steep gradient side of the trough (at 36,335 sec.) is seen to correlate with the sudden increase of precipitated electrons at that time. This is remarkable since these energetic electrons deposit their energy, and thus create ionization, at about 120 km altitude whereas this ion gradient is observed at about 483 km altitude. The ionization increase must have diffused up the magnetic field line to be observed by OVI-18. There is not a one-to-one correspondence between precipitated flux and ionization increase, but such a correspondence cannot really be expected at this high altitude.

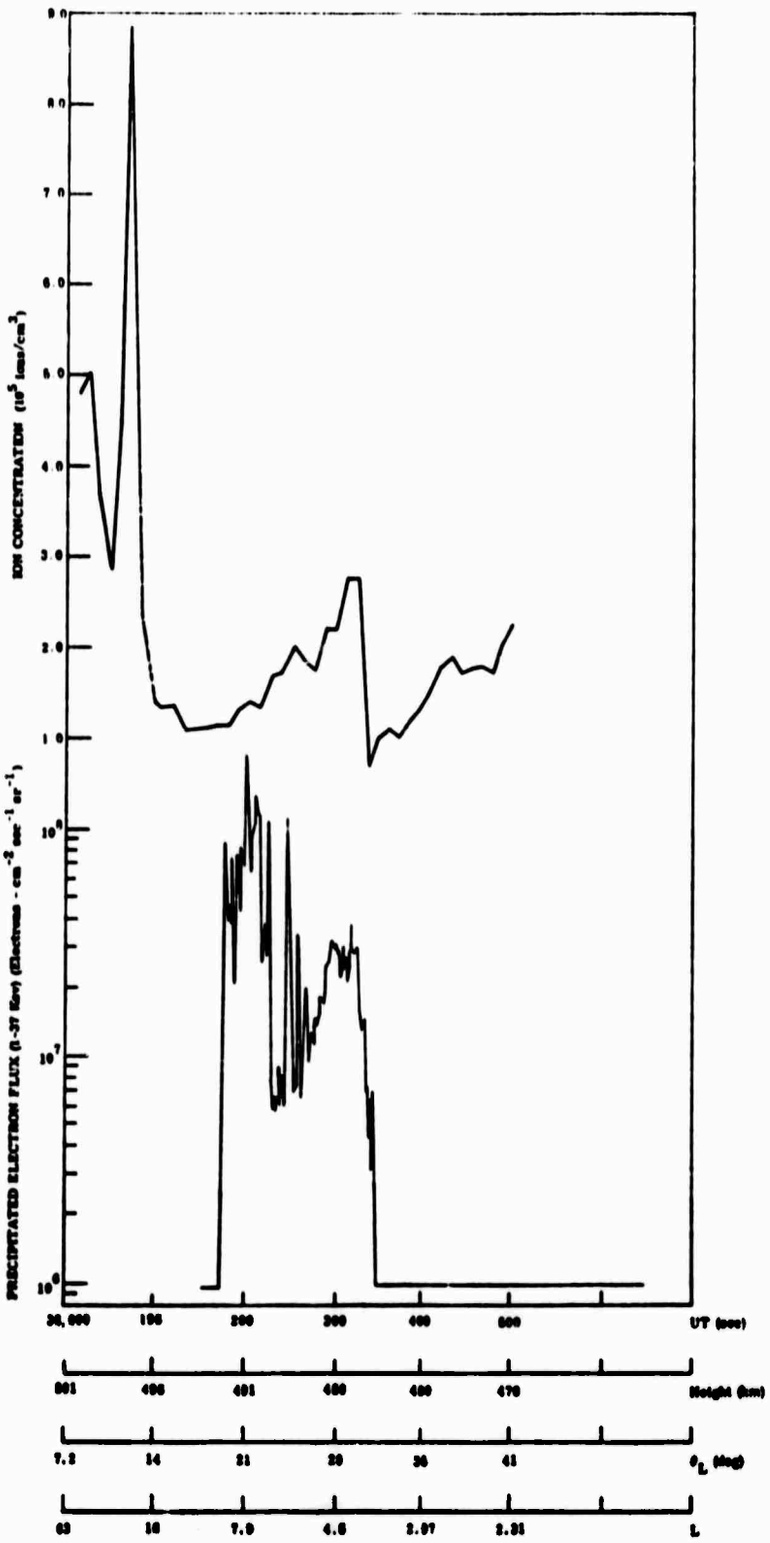

Figure 6-2 North Night Zone Comparison of Ion Concentration and Precipitated Electron Flux from OVI-18 on March 22, 1969, (Acquisition 66)

Figure 6-3 is a plot, similar to Figure 6-2, of ion concentration and precipitated electron flux in the southern night auroral zone on acquisition 66. For reference, this is the third "A" zone from the left in Figure 3-1. The vehicle is at middle latitudes at 38,000 sec. A narrow "mid-latitude trough" is seen in the ionization concentration at 38,100 sec. and then an ionization increase associated with precipitated particles begins and is evident to 38,250 sec., at which time the energetic electrons are no longer observed. The vehicle is in the polar cap region from 38,250 sec. to the end of the plot, which accounts for the low ion concentrations. As with the northern zone, here there is a general correlation of the precipitated particles and an increase in ionization, but there is not a one-to-one correspondence. The measurement altitude (about 540 km) is well above the place where the precipitating particles deposit their energy and create ionization. It does seem quite clear that at least some of the gradients observed in the ionosphere are caused by these energetic precipitating particles.

Figures 6-4 through 6-11 are additional ion concentration/precipitated electron flux plots, similar to Figures 6-2 and 6-3, for other acquisitions of OVI-18. In these plots the precipitated electrons are integrated electron fluxes of electrons with 0.8 to 16 keV energy, and are obtained by adding together the flux measured by four differential detectors covering this energy range. Since the vehicle was tumbling, the detectors used were those in the most favorable position to receive precipitated electrons. Also, in some of these figures there is a bar over some portion of the ion concentration data. This is put there to indicate places where the ion trap may not have a favorable view into

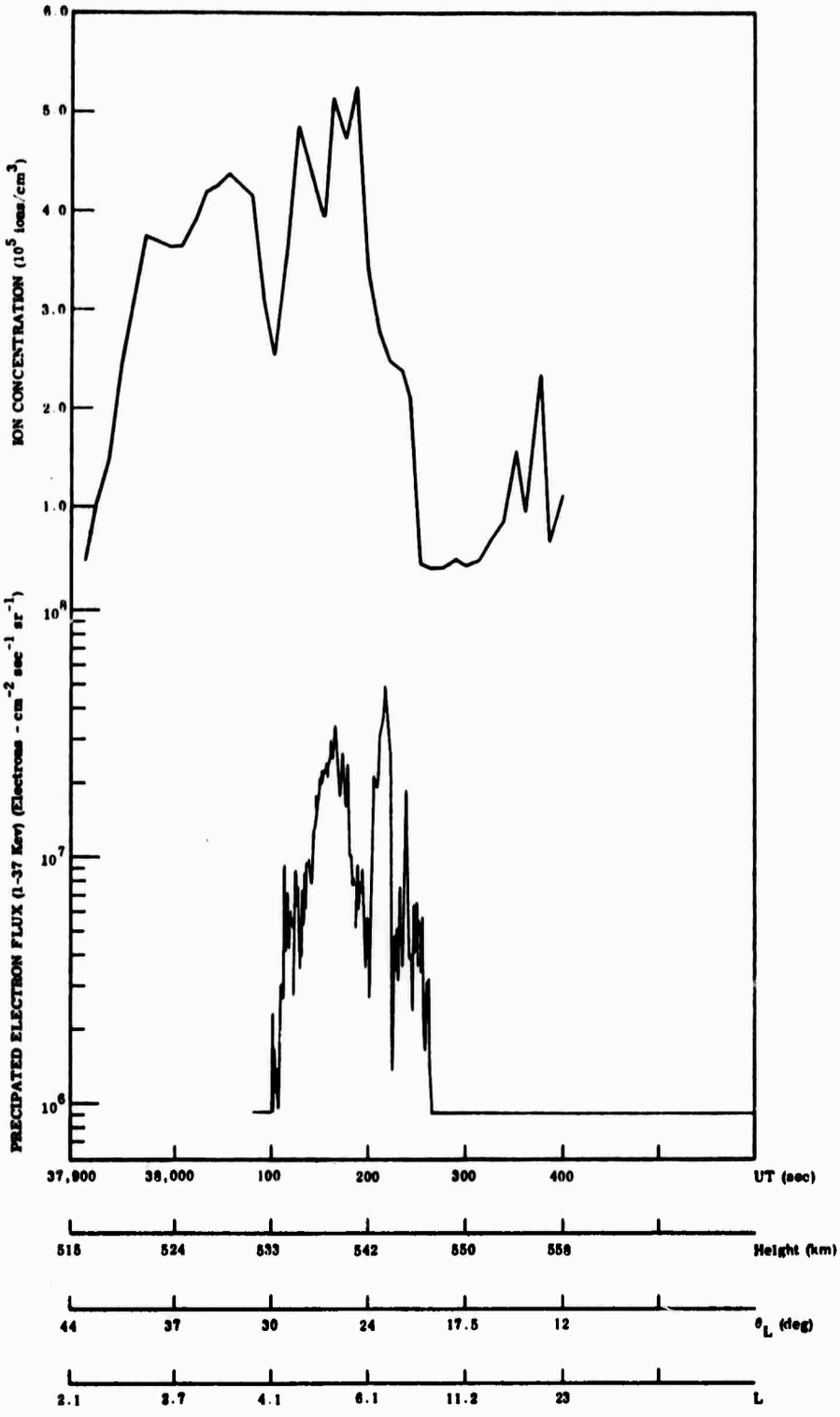

Figure 6-3 South Night Zone Comparison of Ion Concentration and Precipitated Electron Flux from OVI-18 on March 22, 1969, (Acquisition 66)

the velocity vector and that concentration data may not be fully reliable. The portion of the ion concentration curve under the bar is, then, a "best guess" value for that region.

Figure 6-4 is a south night auroral zone pass from acquisition 68, March 22, 1969. The left-hand part of the figure is at middle latitudes and the right-hand part at high latitudes. The mid-latitude trough in ion concentration is seen at about 60850 sec. and shortly after a large gradient increase in ion concentration is seen to correspond with the appearance of precipitated energetic electrons. The pattern of energetic particle precipitation is somewhat more extensive than the pattern of enhanced ionization, which is due probably to the high altitude of the vehicle and the great variability of precipitated particles.

Figure 6-5 is a night north auroral zone pass of the vehicle on March 23, 1969. On the left the spacecraft is in the polar cap (high latitude) region and proceeds through the auroral zone to middle latitudes. The ionization peak near 6950 sec. correlates rather well with a peak of precipitated electron flux, although the flux seen between 6800 and 6900 sec. appear to have little affect on the ionosphere at satellite altitude. The ionospheric mid-latitude trough is seen centered at 7100 sec.

Figure 6-6 is a night north auroral zone pass from acquisition 82, March 23, 1969. It starts (on the left) with the spacecraft in the polar cap region and passes to middle latitudes. The large gradients in ion concentration seen between 58000 sec. and 58125 sec. appear to correlate with energetic electron precipitation in that location, However, the energetic flux near 58200 sec. does not appear to have any affect on the ionosphere at satellite heights.

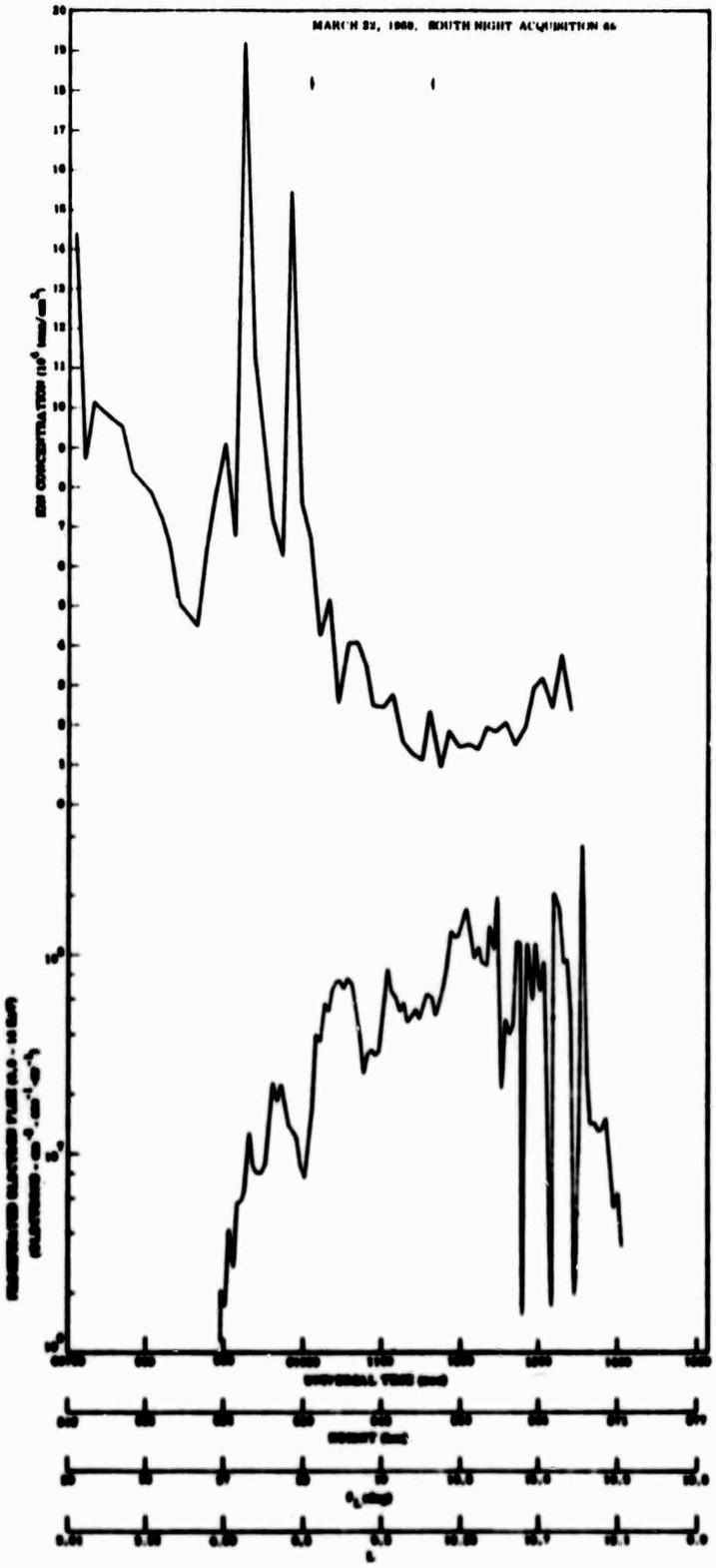

Figure 6-4 South Night Zone Comparison of Ion Concentration and Precipitated Electron Flux from OVI-18 on March 22, 1969 (Acquisition 68)

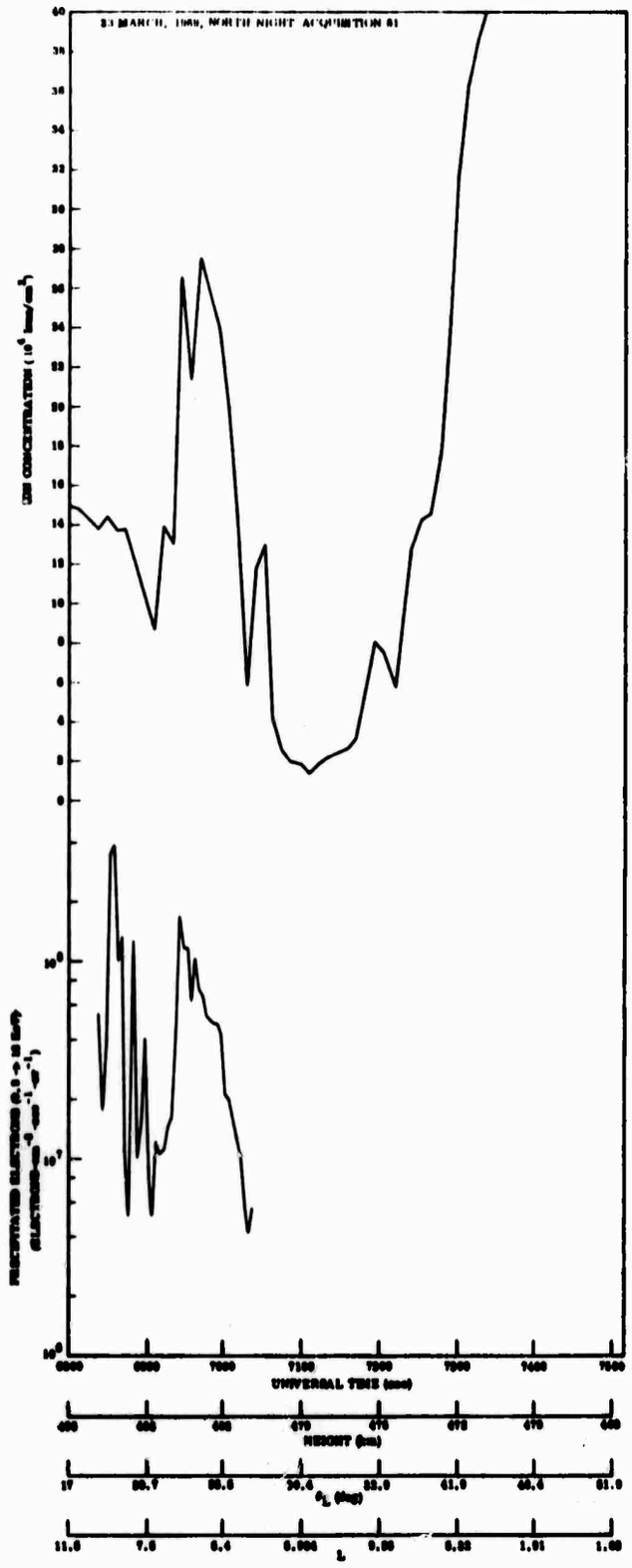

Figure 6-5 Night North Zone Comparison of Ion Concentration and Precipitated Electron Flux from OVI-18 on March 23, 1969 (Acquisition 81)

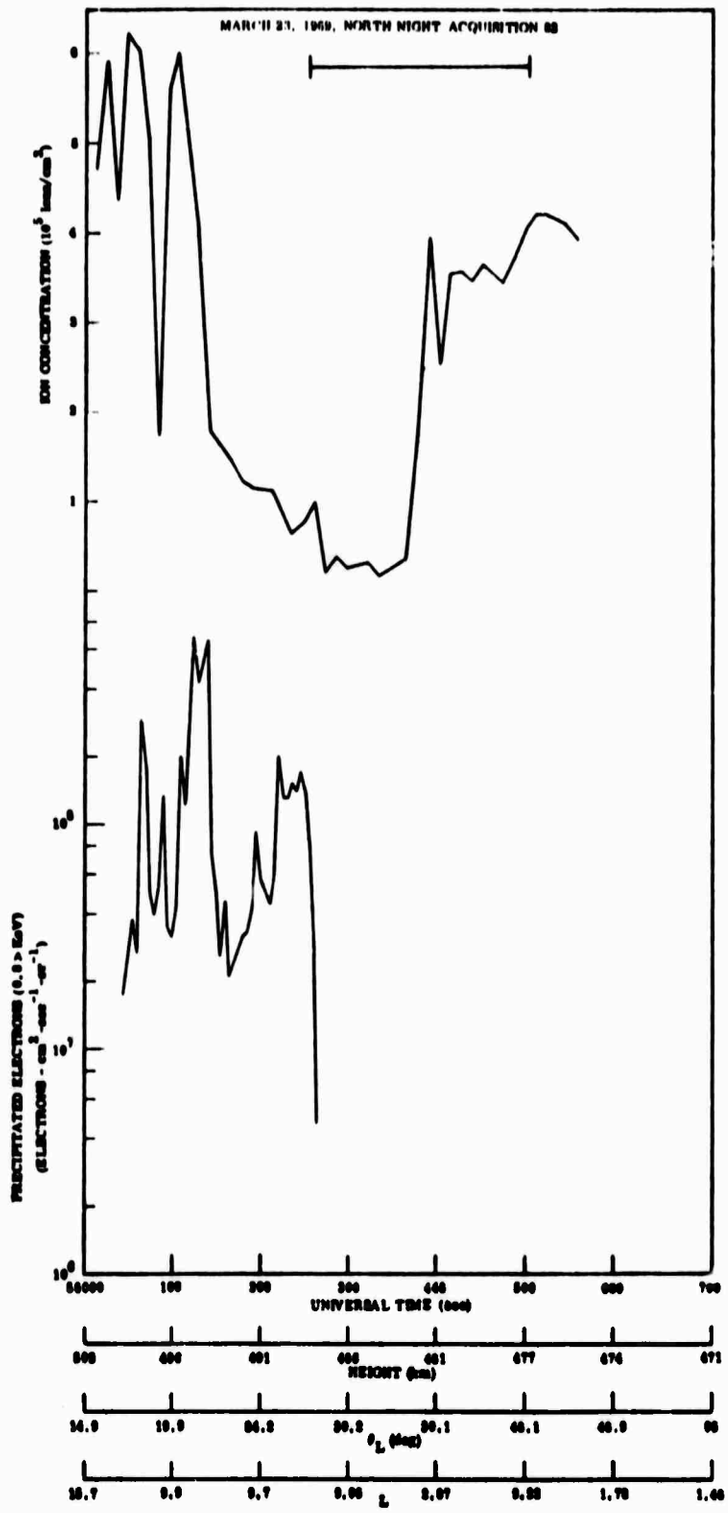

Figure 6-6 Night North Zone Comparison of Ion Concentration and Precipitated Electron Flux from OVI-18 on March 23, 1969 (Acquisition 82)

The next figure, Figure 6-7, is the south auroral zone crossing from this same acquisition, number 82. Here the curve starts with the vehicle at mid-latitudes and passes into the southern polar cap. The mid-latitude trough in the ionosphere is broad and not very deep, extending from 60000 sec. to 60250 sec. The abrupt onset of energetic electrons at about 60125 sec. did not appear to have an affect on the ion concentration at the satellite. The ion concentration gradients seen between 60250 and 60400 sec. do not appear to correlate with the observed precipitated electrons.

Figure 6-8 is the north night auroral zone crossing from acquisition 97, March 24, 1969. The polar region is to the left and the mid-latitude region to the right. Very large gradients are observed in the ion concentration and these seem to relate, at least in a general way, to the pattern of precipitated energetic electrons. The electron flux appears to be located at a higher latitude than the enhanced ionization. A shift of the electron flux curve about 75 seconds to the right would bring the two curves into rather good agreement.

Figure 6-9 is a night north auroral zone crossing from acquisition 128, March 26, 1969. Although ion concentration gradients are observed in the high latitude region (left side of figure), they do not seem to correlate with the location of the observed precipitated electron flux. Also, in this figure the mid-latitude trough seems very broad and shallow.

On this same acquisition (128), data were obtained for the south night auroral zone crossing and is shown in Figure 6-10. In the mid-latitude region, shown on the left of the figure, the ion concentration is relatively high. The mid-latitude trough appears to be the feature shown between 40550 and 40600 sec. UT. The increase in ion concentration

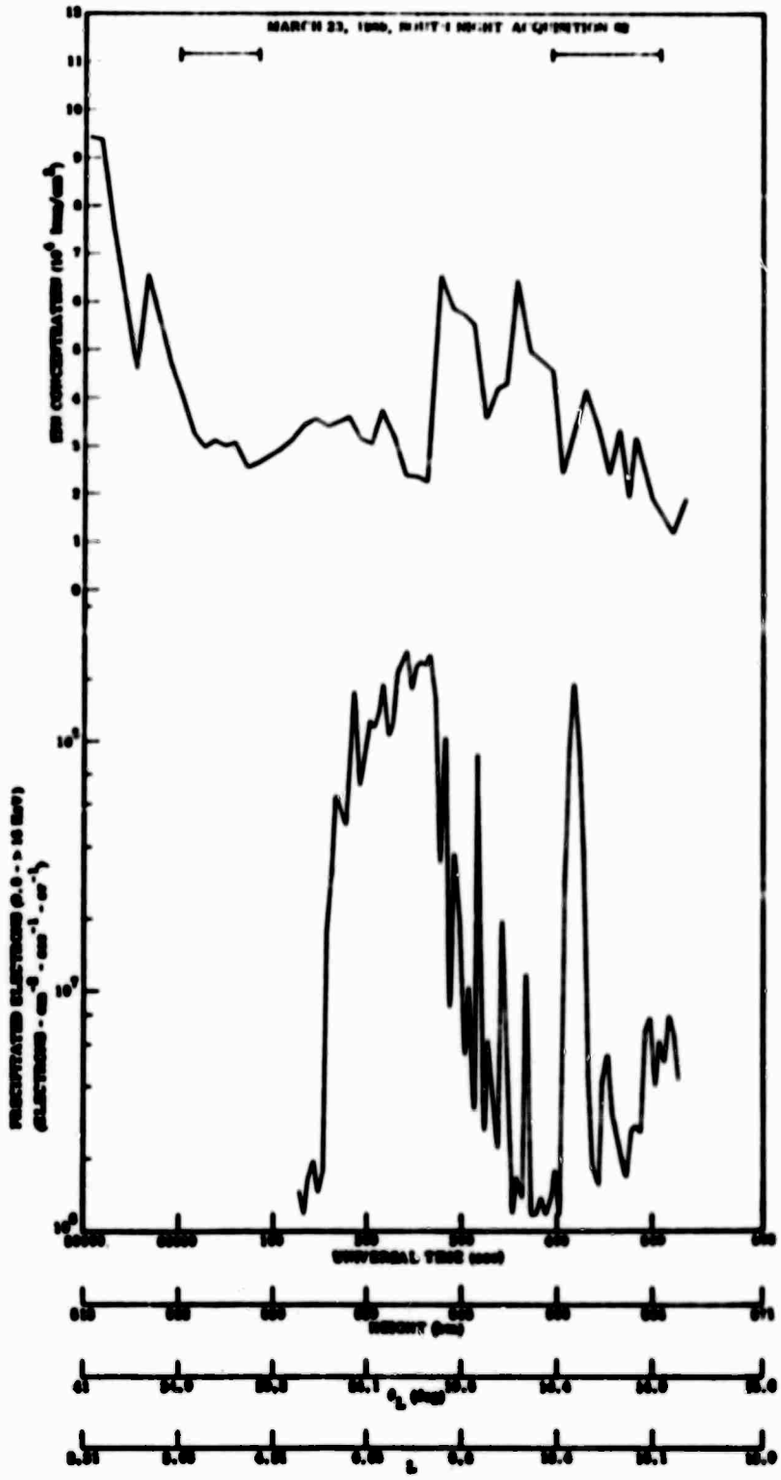

Figure 6-7 South Night Zone Comparison of Ion Concentration and Precipitated Electron Flux from OVI-18 on March 23, 1969 (Acquisition 82)

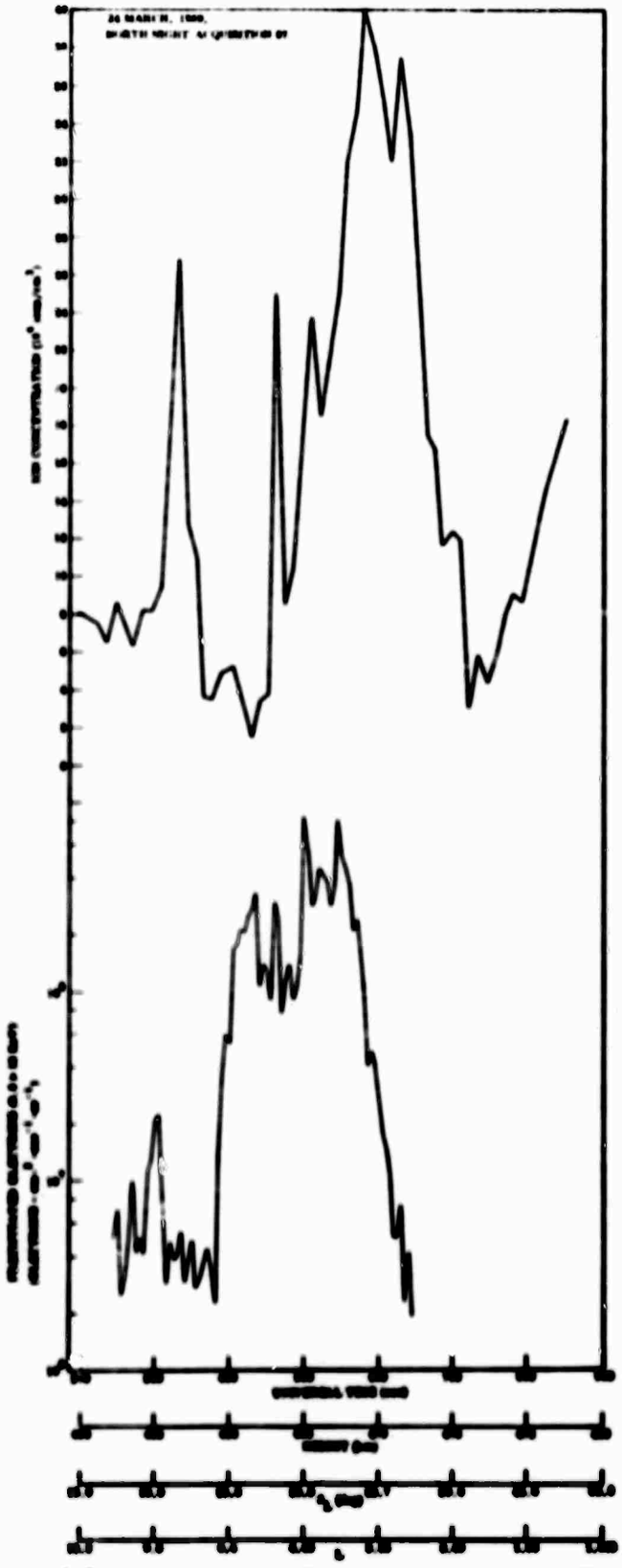

Figure 6-8 North Night Zone Comparison of Ion Concentration and Precipitated Electron Flux from OVI-18 on March 24, 1969 (Acquisition 97)

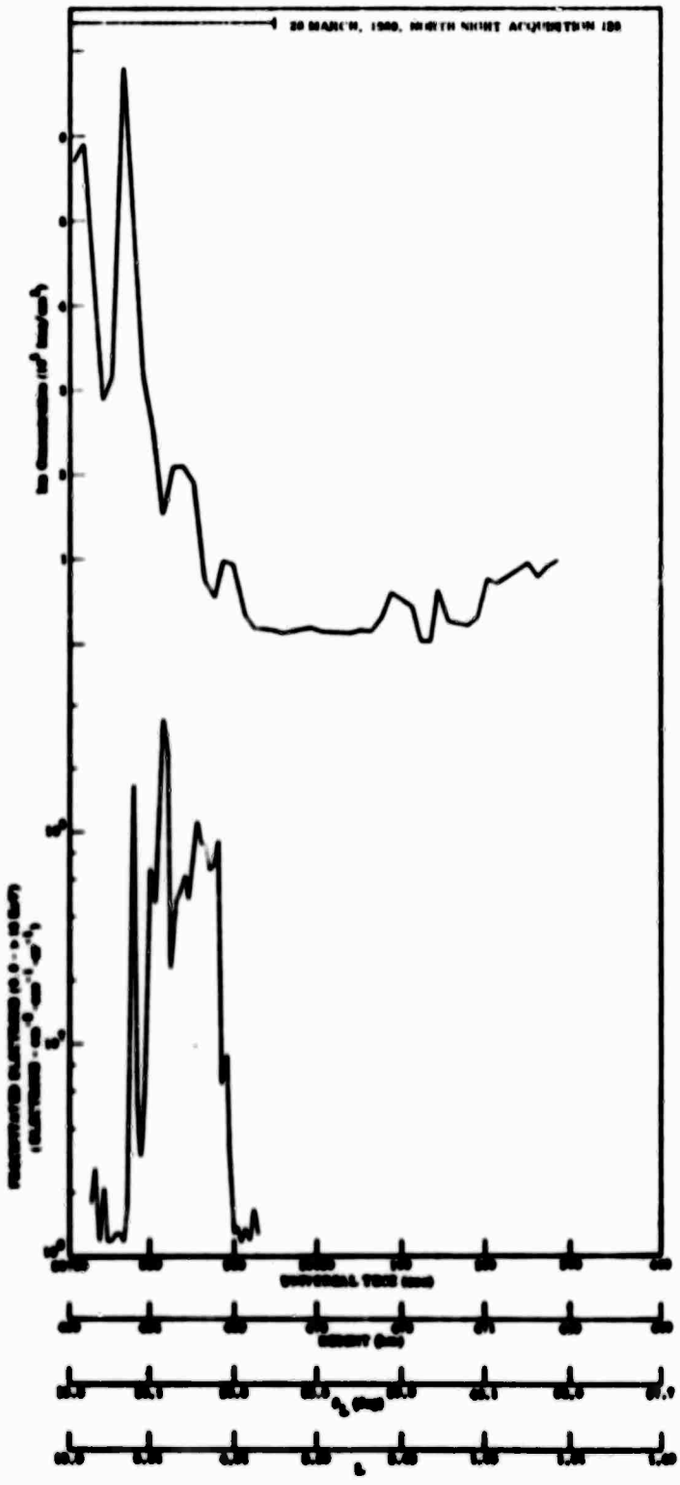

Figure 6-9 North Night Zone Comparison of Ion Concentration and Precipitated Electron Flux from OVI-18 on March 26, 1969 (Acquisition 128)

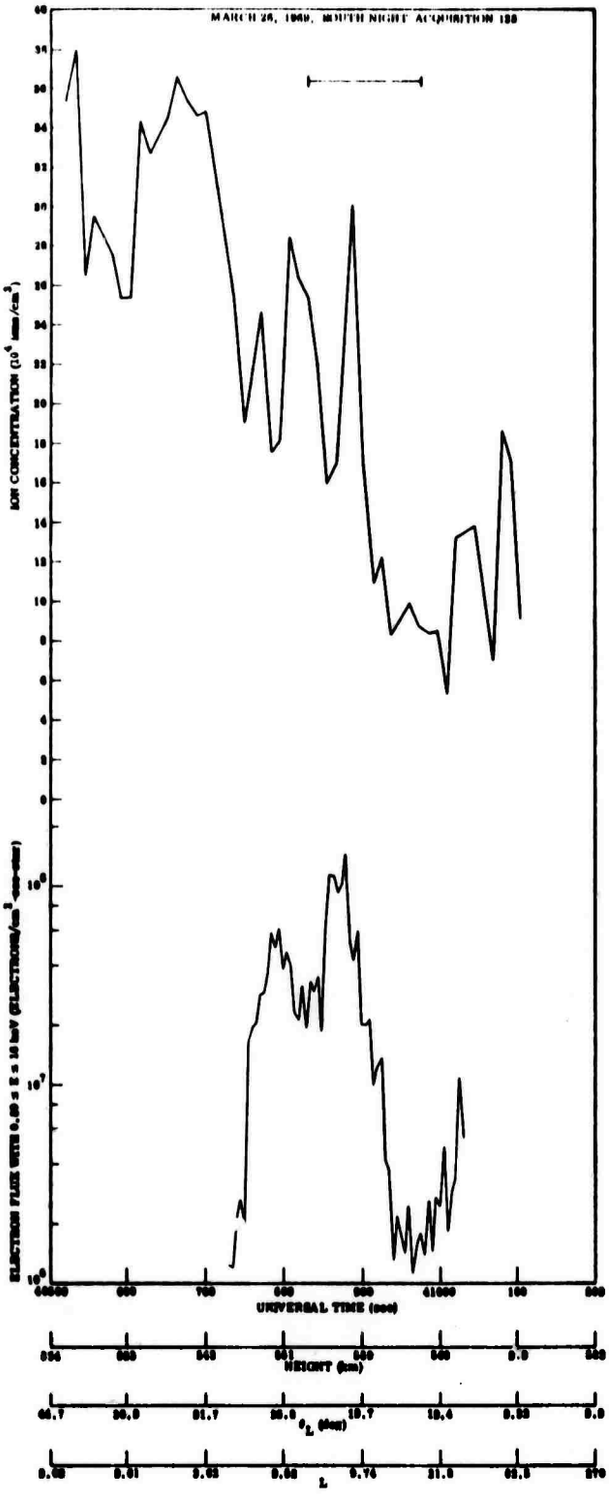

Figure 6-10 South Night Zone Comparison of Ion Concentration and Precipitated Electron Flux from OVI-18 on March 26, 1969 (Acquisition 128)

following that trough seems to preceed the energetic electron input by about 150 seconds. The observation of variable structure in the ion concentration between 40750 and 40900 sec. UT followed by rather low ion density (in the polar cap region) is not unusual.

The final figure in this series of comparisons, Figure 6-11, contains data from acquisition 134, March 26, 1969. This is a north night auroral zone crossing and here we can see a case with a lot of gradients, but one in which the precipitated particles seem to be anti-correlated with the ion concentration. The mid-latitude trough is seen in the right hand portion of the curve at 67440 sec. UT. Moving to the left from that the enhanced peak of ion concentration occurs near the onset of the measurement of energetic electron. However, while the energetic electron flux remains high (moving to the left) the ion concentration soon goes to a deep minimum, rising again near (or in) the polar cap.

The data obtained from OVI-18 were all taken at altitudes above about 450 km which, as we have stated previously, is well above the heights at which the measured precipitated electrons transfer their energy to the atmosphere and ionosphere. So, comparisons of ion gradients and energetic particles can, at best, be loosely qualitative. For the purposes of comparison we have included in this report some ion concentration/energetic particles plots obtained from a DASA auroral package flown on a low altitude, polar orbiting, Air Force Satellite in November 1965 (1965-90A). This data, shown in Figure 6-12, comes from four (4) different passes of the satellite over the northern night auroral zone at altitudes ranging from 195 to 171 km. In this figure ion concentration is plotted on a logarithmic scale as a linear function of time. The precipitated particle

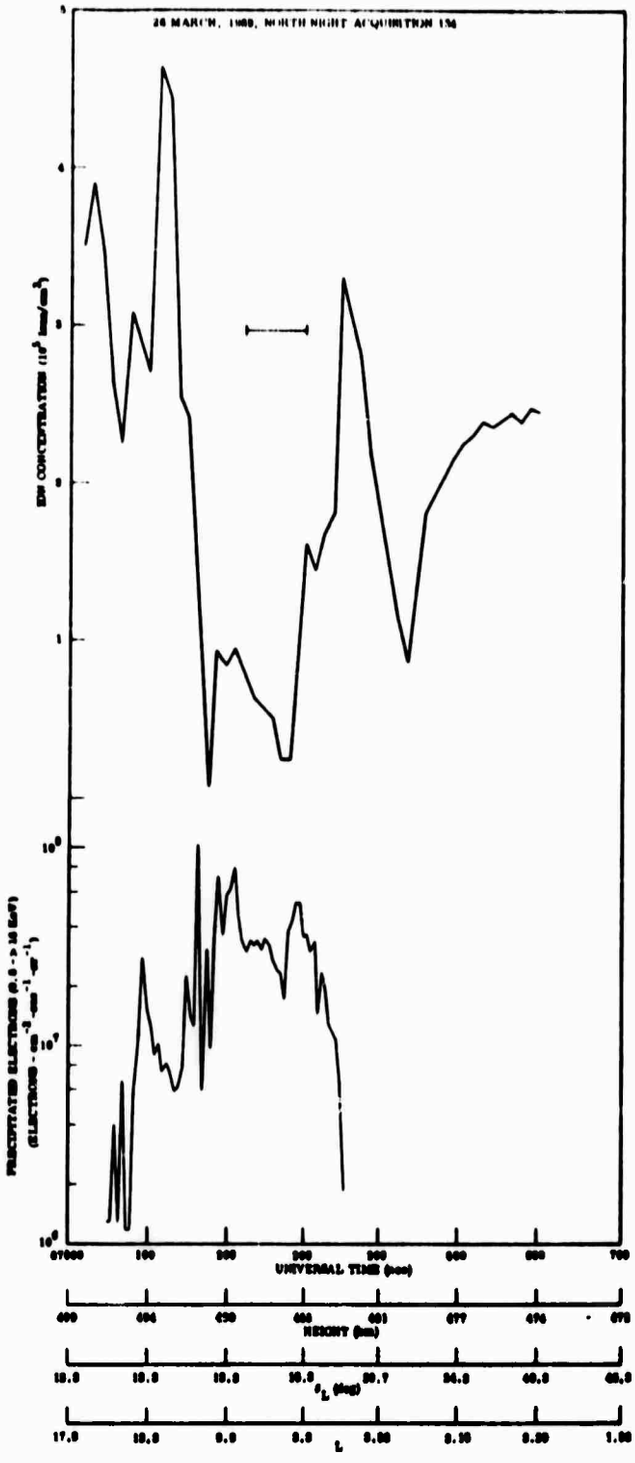

Figure 6-11 North Night Zone Comparison of Ion Concentration and Precipitated Electron Flux from OVI-18 on March 26, 1969 (Acquisition 134)

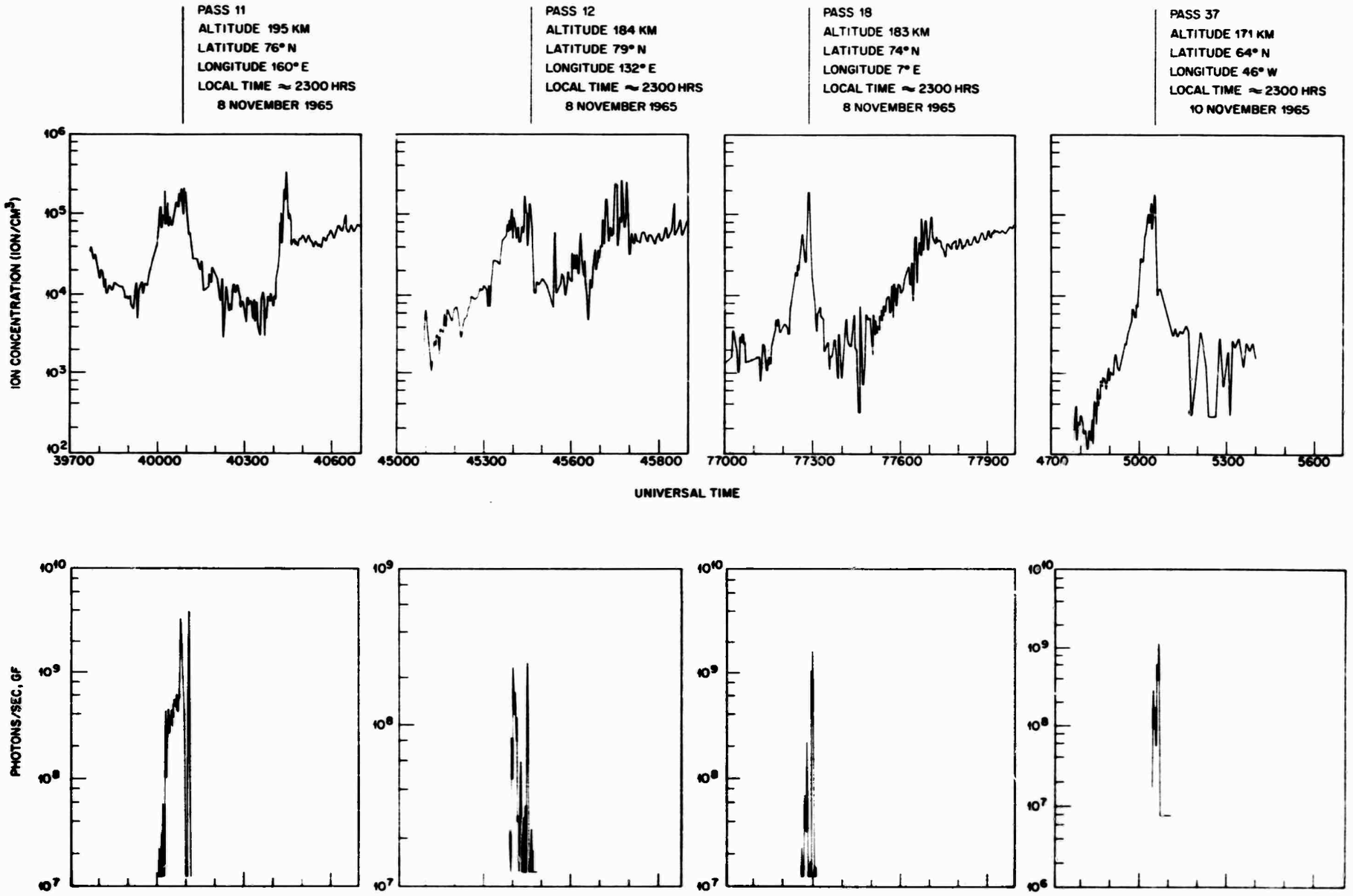

Figure 6-12 Low Altitude North Night Zone Comparisons of Ion Concentration and Precipitated Particles from 1965-90A taken on November 8, 1965.

flux is shown in the lower set of curves and is plotted on an arbitrary logarithmic scale as a linear function of time. The effect of the precipitated particles on the ion concentration is dramatic in each of the four cases shown. The correlation between incoming particle flux and the ionization increase is substantially better in this figure than in the other figures of this section. This is to be expected since the data in Figure 9 are taken at much lower altitudes than that taken in OVI-18. There is still not a one-to-one correspondence between incoming particles and increased ionization since even the 171 km altitude measurement is made somewhat above the region where the majority of the ions are created by the energetic particles.

The conclusion to be drawn from this comparison is that precipitated particles in the nighttime auroral zone give rise to significant ionization gradients at low altitudes and that these effects, although reduced in magnitude, are also seen at altitudes as high as 500 km, well above the F_2 peak in the ionization. At these high altitudes their effect must come about by diffusion up from the altitude of interaction. This creates a time delay in their observation as well as a possible smearing out of certain characteristics. This presumably accounts for why some relatively good correlations are observed (i.e., Figure 6-8) and some almost anti-correlations are also seen (i.e., Figure 6-11).

Section 7

SUMMARY AND CONCLUSIONS

Section 7

Summary and Conclusions

The OVI-18 satellite was launched on 18 March 1969 into a 99° inclination orbit with a 590 km apogee and a 469 perigee. A major portion of the payload was the HIGLO package which contained 13 instruments for measuring ion concentration and temperature, electron concentration and temperature, epithermal electron energy distribution, energy distribution of precipitated electrons and protons, angular and spatial distribution of these same particles, and the intensity and distribution of the very energetic particles which are the cause of Polar Blackout. All of the 13 instruments operated successfully on orbit and provided valuable data. After 18 months of on-orbit operation, 11 of the instruments were still providing excellent data.

Under the present contract detailed analysis has been carried out on the data obtained from satellite acquisitions prior to number 225. Since the satellite failed to achieve its intended earth-oriented condition, but rather performed a complex tumble motion, significant portions of the data were lost due to instruments pointing in ineffective directions. In addition, data analysis was made substantially more difficult for the same reason. Nevertheless, significant results were obtained from the study.

During the first 225 orbits of the spacecraft, there were periods of considerable magnetic activity. In fact, the first orbits of data were obtained during a highly disturbed period. The ion concentration curves for these orbits showed a great deal of horizontal concentration structure

(gradients). A number of the features appeared to be geomagnetically controlled, or oriented, as seen by comparing different orbits that are geomagnetically aligned. The presence of so many gradient features is surprising due to the rather high altitude of the spacecraft and remains an outstanding unresolved item from this study.

On the other hand, many large gradient features were expected to be observed in the high latitude portion of each acquisition. These were seen and the presence of many of them were related to the onset or demise of precipitated energetic electrons in the 0.8 to 16 keV energy range. Correlation in detail between precipitated electrons and the ion concentration gradients was not expected as the satellite measurement of the ions was at an altitude much above the altitude where the precipitated electrons have their greatest affect on the ionosphere. The precipitated particles are very variable, both in intensity and location, and so the ionization effects seen on a given pass are the result of energetic particles deposited at some earlier time. Under such circumstances, it is really surprising that any correlation exist at all. An earlier (1965) flight of a low altitude Air Force satellite gave data with rather high correlation between precipitated energetic electrons and ion concentration enhancements and corroborates the above conclusion.

It is possible to conclude that, at altitudes near 500 km, very significant horizontal gradients do occur in the ionosphere. Most of these gradients appear to be geomagnetically controlled and some them (high latitudes) definitely seem to be created by the precipitated auroral zone particles.